Physics – Uspekhi **66** (10) 1008 – 1024 (2023)

INSTRUMENTS AND METHODS OF INVESTIGATION PACS numbers: 34.20.Gj, 42.50.Md, 42.50.Tx

Polarization echo-spectroscopy in a gas at the transition 0–1

N N Rubtsova, S A Kochubei, E B Khvorostov, V A Reshetov

DOI: https://doi.org/10.3367/UFNe.2022.11.039263

Contents

Abstract. Theoretical and experimental studies of the photon and stimulated photon echo generated at the transition 0–1 of ^{174}Yb atoms are reviewed. Analogues of the phenomena induced by collisions of ^{174}Yb atoms with buffer gas atoms are also considered. The nature of collisions is analyzed.

Keywords: photon echo, polarization, anisotropy of collision relaxation, stimulated photon echo, depolarizing collisions

1. Introduction

Presented below is a study of photon echo, which was predicted by Russian researchers in 1963 [1] and explored experimentally in a solid-state sample in 1964 [2]. Monographs have been published devoted to photon echo, its numerous modifications, and other related coherent nonstationary phenomena [3–7]. Methods for exploring various media are being developed on the basis of the photon echo and its modifications. Experimental implementations of photon echo methods involve radiation pulses of various durations (ranging from nano- to femtoseconds) and employ exciting radiation of various degrees of coherence and various spectral ranges (from the far infrared to X-ray). The properties of the photon echo turn out to be so exciting that methods for mathematical processing of optical data are being developed on their basis; information about optical phase and quantum memory devices on gas and solid-state storage media can be found in [6, 7]. Some aspects of the currently fashionable field of quantum information science use the properties of the photon echo.

The simplest way to generate a photon echo (PE) in a gas is to direct two light pulses, resonant to a inhomogeneously broadened allowed optical transition of the gas medium, to the sample under study. A simplified description of the photon echo can be derived in a gas model of two-level atoms. The model of two-level atoms has attracted the attention of researchers, also in relation to the interpretation of spin and photon echo phenomena [4, 8, 9].

In the gas model of two-level atoms, inhomogeneous broadening is provided by the Doppler effect, due to which the transition frequency ω_0 for gas particles having velocity $\mathbf{v}$ is transformed into $\omega_0 + \mathbf{kv}$, where $\mathbf{k}$ is the wave vector of radiation. In this model, it is easy to determine a set of the conditions required for obtaining a photon echo: low gas pressure, which ensures inhomogeneous broadening of the line; and optimal areas of resonant radiation pulses $\theta_i = T_i\Omega_i$, where T_i is the duration of the pulse (often assumed to be rectangular), and $\Omega_i = dE_i/\hbar$ represents the frequency of induced transitions determined by the matrix element of the dipole transition d and the strength of electric field E_i of the light wave of the ith pulse. For the first pulse, the optimal area $\theta_1 = \pi/2$ provides maximum polarization of the medium created by the first pulse. For the simplest case of a gas of two-level atoms, the action of a resonant light pulse in the direction of the Z-axis generates polarization of the gaseous medium; the phase of each emitter in time t, measured from the first pulse, varies according to the law $(\omega_0 + kv_z)t$. A set of emitters with different speeds v_z, initially phased due to the

N N Rubtsova [1,*], **S A Kochubei** [1], **E B Khvorostov** [1], **V A Reshetov** [2]
[1] Rzhanov Institute of Semiconductor Physics,
Siberian Branch of the Russian Academy of Sciences,
prosp. Lavrent'eva 13, 630090 Novosibirsk, Russian Federation
[2] Togliatti State University,
ul. Belorusskaya 14, 445020 Togliatti, Russian Federation
E-mail: [*] rubtsova@isp.nsc.ru

Received 8 August 2022, revised 10 November 2022
Uspekhi Fizicheskikh Nauk **193** (10) 1071 – 1089 (2023)
Translated by M Zh Shmatikov

short duration of the light pulse, undergoes dephasing over time according to the law kv_zt. For the second pulse of resonant radiation entering the medium with a delay τ after the first pulse, the optimal area is $\theta_2 = \pi$. After interaction with the second radiation pulse, the polarization phase sign is completely reversed for each group of velocities (changes from the value $kv_z\tau$ to $-kv_z\tau$). Finally, a photon echo is formed at a time approximately equal to 2τ. Another important condition for the formation of a photon echo in a gas is the small influence of collisions. Both inelastic collisions of active particles and elastic collisions, which significantly alter the velocity of translational motion, lead to attenuation of PE signals.

The evolution of Doppler phases shown in Fig. 1 gives an idea of the mechanisms that form a photon echo in this simplest model. Elastic collisions that significantly change the projection of the translational motion velocity v_z should apparently result in the disappearance of the contribution from the corresponding phase trajectories and, consequently, to additional attenuation of the photon echo signal. Thus, for PE, elastic collisions with a significant change in velocity (referred to as velocity changing collisions) perform as extinguishing collisions. As for elastic collisions with a small change in the projection of the translational velocity v_z, their contribution is manifested in the deviation from the exponential decay law of the PE signal as a function of delay time τ, implying that they also lead to additional attenuation in the PE kinetics, which was observed experimentally for molecules [10, 11] and atoms [12] using various versions of the photon echo.

The second best known type of coherent echo response is stimulated photon echo (SPE). To form this echo, three pulses of resonant radiation are used. The first, as in the case of PE formation, creates a nonequilibrium polarization of the medium; its optimal area is also $\theta_1 = \pi/2$. The second pulse, arriving with delay τ_{12} after the first one, does not reverse the sign of the Doppler phases, as occurs during the formation of the PE, but only converts nonequilibrium polarization into

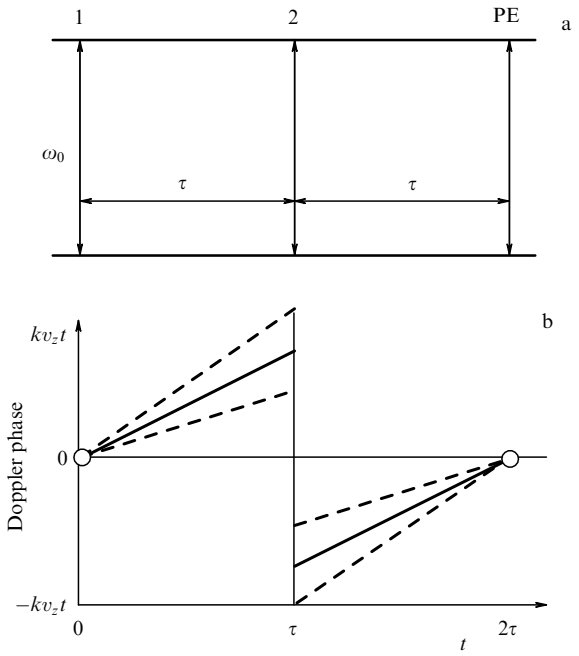

Figure 1. (a) Sequence of resonant radiation pulses forming PE and (b) Doppler phase evolution.

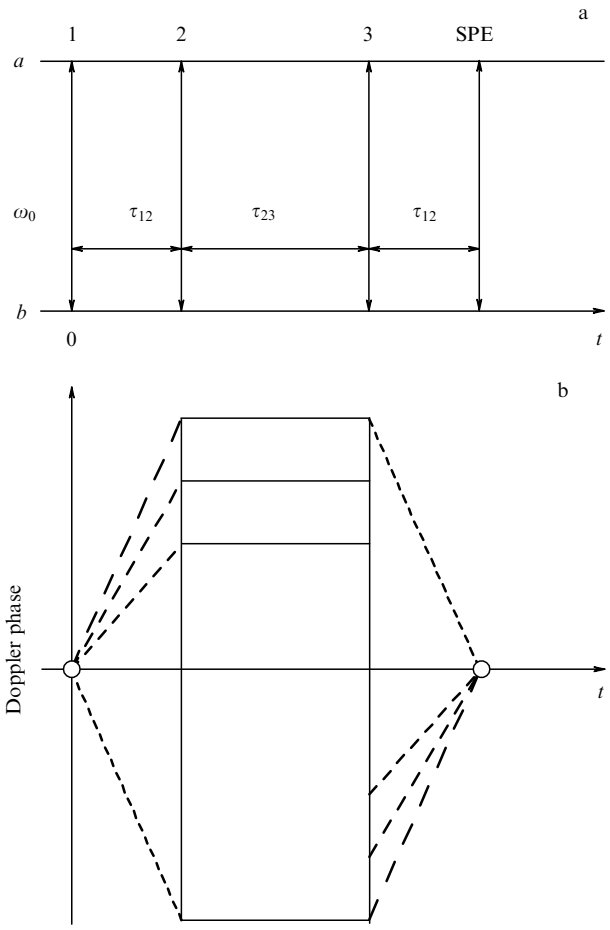

Figure 2. (a) Sequence of resonant radiation pulses forming SPE and (b) Doppler phase evolution.

nonequilibrium level populations. The optimal area for this pulse is $\theta_2 = \pi/2$. Doppler phases turn out to be 'preserved' in the level populations for the time between the end of the second pulse and the arrival of the third radiation pulse, i.e., for the delay time τ_{23}. The third pulse of resonant radiation with an area of $\theta_3 = \pi/2$ converts nonequilibrium populations into polarization of the medium and reverses the Doppler phase signs. Therefore, after delay τ_{12} after the end of the third pulse, a coherent response is formed — a stimulated photon echo. A simplified diagram of SPE formation is displayed in Fig. 2.

The process of SPE formation can be considered an analogue of PE, in which the reversal of the emitter phase sign is time-separated into two interactions that occur with the second and third pulses. The time interval τ_{23} corresponds to the storage time of data in the above-mentioned 'frozen' Doppler phases. In the approximation of small areas of exciting pulses, the electric field of the SPE response linearly depends on the electric fields of the exciting pulses; therefore, the temporal shape of the second exciting pulse is reproduced in the SPE signal without distortion. Due to this, the entire process can be interpreted as recording optical information in the form of a temporal form of the second 'recording' pulse, storing it during the time interval τ_{23}, and reproducing information after the third 'reading' pulse is applied with a delay τ_{12} after the end of the third pulse (usually in such experiments, $\tau_{12} \ll \tau_{23}$). Stimulated photon echo was used as the basis for the development of systems for recording and

storing optical data [13]. The remark about the contribution of elastic collisions involving a change in velocity to the attenuation of the coherent response fully applies to the SPE phenomenon. Only those resonant particles (atoms or molecules) that have been exposed to all three pulses of exciting radiation can contribute to the SPE signal formation. Elastic scattering with a change in translational motion velocity operates throughout the entire period of time from the end of the first exciting pulse to the moment when the coherent response is formed, so its contribution to the attenuation of the SPE can be significant.

The approximation of a two-level-atom gas was an important stage in the development of the theory of photon echo in gases, indicating some continuity with the spin echo phenomenon. However, even in such a simplified approach, there are features of the photon echo that distinguish it from the spin echo. For a spin echo recorded in the microwave range for electron spins and in the radio frequency spectrum range for nuclear spins, the resonant radiation wavelength exceeds the dimensions of a sample. Therefore, the issue of spatial synchronization of emitters is not relevant. Today, photon echo experiments are carried out in various spectral regions, from infrared to ultraviolet, and in a variety of environments. In this case, the sample dimensions significantly exceed the resonant radiation wavelength, and the requirements for spatial synchronism arise for each modification of the photon echo. The variety of PE modifications is determined by the number of radiation pulses that form a coherent echo-type response, the scheme of operating energy levels, the relative arrangement of the wave vectors of the exciting pulses, and the type of excitation of the transition under study (resonant absorption or stimulated Raman scattering-type excitation).

The model of a two-level-atom gas is not applicable to the interpretation of experiments that examine the polarization properties of the photon echo. Taking into account the degeneracy of resonant levels [5, 14] made it possible not only to provide a correct interpretation of the polarization properties of the photon echo in gases but also to propose a technique for studying depolarizing collisions, which is an important relaxation channel of atomic collisions.

The purpose of this review is to present methods for the experimental study of depolarizing collisions using the example of ^{174}Yb $^1S_0$ ($6s^2$) $\leftrightarrow$ $^3P_1$ (6s6p) transition under conditions of collisions of ^{174}Yb atoms with noble gas atoms.

2. Photon echo at the transition 0–1

2.1 On the polarization of a photon echo

For an optically allowed transition between levels with total angular momenta of the levels J_a and J_b, the photon echo is the sum of coherent responses of transitions among all magnetic sublevels. In the absence of collisions, PE polarization depends on the polarization of the exciting pulses of resonant radiation, the type of transition, and the specific values of the angular momenta of the operating levels of the transition under study. In the approximation of small areas of resonant radiation pulses that form PE, the PE polarization properties were predicted in [5, 14]. For some vibrational-rotational transitions of molecules, theoretical predictions for the limiting case $J_i \gg 1$ were confirmed experimentally [15].

For some transitions with small angular momenta of operating levels, the PE polarization has a simpler form. In particular, for the 0–1 transition, the photon echo is polarized in the same way as the second pulse of resonant radiation [5]. At the 0–1 transition, the PE polarization properties do not depend on the areas of the exciting pulses. If both pulses of exciting resonant radiation are polarized linearly, with an angle ψ between their polarization vectors, the amplitude of the electric field of the photon echo varies according to the $E_e \propto \cos\psi$ law, and the direction of the PE polarization vector coincides with that of the polarization vector of the second pulse of resonant radiation. These PE properties were verified experimentally using the example of a 0–1-type transition in ^{174}Yb atoms under conditions where the influence of depolarizing collisions could be neglected.

Among the most interesting polarization properties of PE at the 0–1 transition, the absence of PE should be noted in two cases: for resonant radiation pulses polarized linearly and mutually orthogonally, and when two exciting radiation pulses are polarized in a circle opposite to each other (right-handed and left-handed polarization). It should be emphasized that the PE polarization properties described above should manifest themselves in the absence of depolarizing collisions.

2.2 Formation of a photon echo at the 0–1 transition, taking into account depolarizing collisions

We now consider the formation of a photon echo at a transition with angular momenta of levels $J_a = 0 \rightarrow J_b = 1$ under the action of two pulses of resonant laser radiation with durations T_1 and T_2 and with a delay τ between them. The electric field strength of these radiation pulses propagating along the Z-axis with a carrier frequency ω is represented in the form

$$\mathbf{E}_n = e_n \mathbf{l}_n \exp\left[-\mathrm{i}(\omega t - kz)\right] + \text{c.c.}\,, \quad n = 1, 2\,, \tag{1}$$

where e_n and $\mathbf{l}_n$ are the amplitudes and unit polarization vectors of these pulses. We assume that all pulses are significantly shorter than all relaxation times corresponding to a homogeneous broadening of the spectral line. Then, the dynamics of the interaction of an atom with the radiation of the nth laser pulse can be represented by the equation for the density matrix $\hat{\rho}$:

$$\dot{\hat{\rho}} = \mathrm{i}[\hat{V}_n, \hat{\rho}]\,, \quad \hat{V}_n = \frac{\Delta}{2}(\hat{P}_b - \hat{P}_a) + \frac{|d|e_n}{\hbar}(\hat{g}_n + \hat{g}_n^+)\,. \tag{2}$$

Here, $\Delta = kv_z - \omega + \omega_0$ is the detuning of the laser radiation frequency from resonance, $\hat{P}_{a,b}$ are projection operators onto subspaces corresponding to atomic levels a, b, $d = d(J_a, J_b)$ is the reduced matrix element of the electric dipole moment operator for the transition $J_a \rightarrow J_b$, and $\hat{g}_n = (\hat{\mathbf{g}}\mathbf{l}_n^*)$, where $\hat{\mathbf{g}}$ is the operator of the dimensionless electric dipole moment for the transition $J_a \rightarrow J_b$, and the matrix elements of its circular components are expressed through the $3J$ Wigner symbols:

$$(\hat{g}_q)^{ab}_{\mu m} = (-1)^{J_a - \mu} \frac{d}{|d|} \begin{pmatrix} J_a & 1 & J_b \\ -\mu & q & m \end{pmatrix}. \tag{3}$$

The solution to Eqn (2) can be expressed using the evolution operator $\hat{S}_n = \exp(\mathrm{i}\hat{V}_n T_n)$. The explicit form of evolution operator (2) is given in [16]. Initially, the atom is in the ground state with the density matrix $\hat{\rho}(0) = \hat{P}_a$. The first laser pulse creates atomic coherence on the transitions $m_a = 0 \rightarrow m_b = q = \pm 1$, which is represented by off-diagonal elements of the

density matrix

$$\rho_{0q}^{ab}(T_1) = (\hat{S}_1)_{00}^{aa}(\hat{S}_1^+)_{0q}^{ab} \sim l_{1,-q}^*\,, \tag{4}$$

where $l_{n,q}$ ($q = 0, \pm 1$) are the circular components of the unit vector $\mathbf{l}_n$ of the polarization of the nth exciting pulse.

Within the time interval between pulses, the evolution of the off-diagonal matrix elements responsible for the formation of the photon echo is driven by the frequency detuning Δ of the laser radiation from the center of the transition, taking into account the Doppler effect and relaxation during collisions. Taken into account for an atom are the spontaneous decay of an excited level with rate $\gamma^{(1)}$ and elastic depolarizing collisions, which do not change the atom velocities, but lead to transitions between Zeeman sublevels of resonant atomic levels [5]. For the transition $J_a = 0 \to J_b = 1$, these collisions of the active atom with the buffer atoms are characterized by two different complex relaxation rates, which depend on the modulus of the atom velocity v: $\Gamma_0(v) + \mathrm{i}\Delta_0(v)$ for the dipole moment component collinear with the atom velocity and $\Gamma_1(v) + \mathrm{i}\Delta_1(v)$ for the dipole moment component orthogonal to the atomic velocity vector [17]. In a reference frame in which the Z'-axis is directed along the atomic velocity vector $\mathbf{v}$, atomic coherence $\rho_{0q}'^{ab}(T_1)$ decays exponentially. Equations representing the evolution of matrix elements $\rho_{0q}^{ab}(T_1)$ in a laboratory reference frame with the Z-axis parallel to the wave vector of laser pulses can be obtained [16] using rotation matrices,

$$\rho_{0q}^{ab}(\tau) = \exp(-\gamma\tau + \mathrm{i}\delta\tau) \sum_{q'} R_{qq'}(\tau) \exp\left[\mathrm{i}(q'-q)\phi\right] \rho_{0q'}^{ab}(T_1)\,, \tag{5}$$

where

$$\gamma = \gamma^{(1)} + \frac{\Gamma_1(v) + \Gamma_0(v)}{2}\,,$$

$$\delta = kv\cos\xi + \omega_0 - \omega - \frac{\Delta_1(v) + \Delta_0(v)}{2}\,,$$

while the resolution matrix

$$\hat{R}(\tau) = \exp\left(\frac{\lambda\tau}{2}\right)\hat{1} - \sinh\left(\frac{\lambda\tau}{2}\right)\hat{\Upsilon}, \tag{6}$$

$$\hat{\Upsilon} = \begin{pmatrix} \sin^2\xi & -\frac{1}{\sqrt{2}}\sin(2\xi) & -\sin^2\xi \\ -\frac{1}{\sqrt{2}}\sin(2\xi) & 2\cos^2\xi & \frac{1}{\sqrt{2}}\sin(2\xi) \\ -\sin^2\xi & \frac{1}{\sqrt{2}}\sin(2\xi) & \sin^2\xi \end{pmatrix}, \tag{7}$$

is determined by the difference between the relaxation rates

$$\lambda = \Gamma_0(v) - \Gamma_1(v) + \mathrm{i}\left[\Delta_0(v) - \Delta_1(v)\right]$$

and depends on the angle between the atomic velocity vector and the wave vector of laser radiation ξ, while the dependence of the solution to Eqn (5) on the velocity angle ϕ is explicitly expressed by the exponential factor $\exp\left[\mathrm{i}(q'-q)\phi\right]$. For a nonzero difference in relaxation rates λ, the resolution matrix $\hat{R}(\tau)$ contains nonzero nondiagonal elements of coherence transfer $R_{-1,1}(\tau)$ and $R_{1,-1}(\tau)$, which describe the mutual transfer of coherence between transitions $m_a = 0 \to m_b = -1$ and $m_a = 0 \to m_b = 1$ under the effect of depolarizing collisions.

The second laser pulse reverses the Doppler dephasing according to the solution of Eqn (2):

$$\rho_{0q}^{ab}(T_2) = \sum_{q'} (\hat{S}_2)_{0q'}^{ab} \rho_{q'0}^{ba}(\tau) (\hat{S}_2^+)_{0q}^{ab} \sim \exp(-\mathrm{i}\delta\tau)\,. \tag{8}$$

After the second pulse passes through the gaseous medium, the evolution of the atom is described by the same equation (5), where T_1 should be replaced by T_2 and τ by $t' = t - z/c - T_1 - \tau - T_2$. The electric field strength of the echo signal, which is obtained from the Maxwell's equation, is determined by density matrix components $\rho_{q0}^{ba}(\mathbf{v}, t')$ at time t':

$$\mathbf{E}^{\mathrm{e}} = \mathbf{e}^{\mathrm{e}}(t') \exp\left[-\mathrm{i}(\omega t - kz)\right] + \mathrm{c.c.}\,, \tag{9}$$

$$e_q^{\mathrm{e}}(t') = \mathrm{i}e_0 \int \rho_{-q0}^{ba}(\mathbf{v}, t') f(\mathbf{v})\,\mathrm{d}\mathbf{v}\,, \quad e_0 = \frac{2\pi\omega L n_0 d}{c\sqrt{3}}\,, \tag{10}$$

where $e_q^{\mathrm{e}}(t')$ are the circular components of the vector $\mathbf{e}^{\mathrm{e}}(t')$, L is the gaseous-medium length, n_0 is the concentration of resonant atoms, and $f(\mathbf{v})$ is the Maxwellian velocity distribution function. Further we assume that the relaxation rates weakly depend on the velocity modulus v, so

$$\Gamma_q(v) \approx \Gamma_q(u)\,, \quad \Delta_q(v) \approx \Delta_q(u)\,,$$

where $u = \sqrt{2k_{\mathrm{B}}T/m}$ is the average thermal velocity of the atom. Then, in the case of exact resonance $\omega = \omega_0 - (\Delta_0 + \Delta_1)/2$, after integration over the velocity angles ϕ from Eqn (10) for two echo polarization components $e_n^{\mathrm{e}}(t') = \mathbf{e}^{\mathrm{e}}(t')\mathbf{s}_n^*$, where $\mathbf{s}_n$ ($n = 1, 2$) is a pair of arbitrary mutually orthogonal vectors in the XY plane, we obtain the following formula:

$$e_n^{\mathrm{e}}(t') = e_0 \exp(-2\gamma\tau) \int_{-1}^{1} \mathrm{d}z\, G(z, t' - \tau) H_n(z, \tau)\,, \tag{11}$$

where $z = \cos\xi$,

$$G(z, t' - \tau) = \int_0^\infty x^2 \exp\left[-x^2 - \mathrm{i}ku(t' - \tau)xz\right] F(xz)\,\mathrm{d}x \tag{12}$$

contains integration over the absolute value of velocity $x = v/u$; function $F(xz)$ is defined by the relations

$$F(xz) = \frac{2}{\sqrt{\pi}}\, Q_1\, \frac{\theta_1\theta_2^2}{\Omega_1\Omega_2^2} \sin\left(\frac{\Omega_1}{2}\right) \sin^2\left(\frac{\Omega_2}{2}\right),$$

$$Q_1 = \cos\left(\frac{\Omega_1}{2}\right) + \mathrm{i}\,\frac{kuT_1xz}{\Omega_1} \sin\left(\frac{\Omega_1}{2}\right),$$

with

$$\Omega_n = \sqrt{(kuT_n)^2 x^2 z^2 + \theta_n^2}\,, \quad \theta_n = \frac{2|d|e_n T_n}{\sqrt{3}\hbar}\,,$$

while

$$H_n(z, \tau) = \sum_{q,\sigma,k} R_{q,q-k}^*(\tau) R_{\sigma,\sigma-k}(\tau) (L_n)_{q\sigma k}\,, \tag{13}$$

$$(L_n)_{q\sigma k} = (s_{n,-q})^* (l_{2,k-q})(l_{2,-\sigma})(l_{1,k-\sigma})^*\,.$$

Then, as follows from Eqns (11)–(13),

$$\mathbf{e}^{\mathrm{e}}(t')\mathbf{s}_n^* \sim H_n(z,\tau) = (\mathbf{l}_2\mathbf{s}_n^*)\,(\mathbf{l}_2\mathbf{l}_1^*).$$

Since $\mathbf{s}_n$ $(n = 1, 2)$ are two arbitrary mutually orthogonal unit vectors, in this case, the polarization of the usual photon echo coincides with that of the second exciting pulse: $\mathbf{e}^{\mathrm{e}}(t') \sim \mathbf{l}_2$. The echo amplitude vanishes for orthogonal polarizations of the exciting pulses $(\mathbf{l}_2\mathbf{l}_1^* = 0)$ and reaches its maximum when the polarizations of both exciting pulses coincide.

2.3 Polarization properties of a collision induced photon echo

We assume that the difference $\lambda = \Gamma_0 + \mathrm{i}\Delta_0 - \Gamma_1 - \mathrm{i}\Delta_1$ between two relaxation constants due to depolarizing collisions is much less than the homogeneous width of the spectral line γ, $|\lambda| \ll \gamma$, so, for a conventional photon echo, the resolution matrix of Eqn (6) can be considered the identity matrix: $R_{qq'}(\tau) = \delta_{qq'}$. Then, as follows from Eqn (13),

$$H_n(z,\tau) = (\mathbf{l}_2\mathbf{s}_n^*)(\mathbf{l}_2\mathbf{l}_1^*)\,,$$

which implies that the polarization of a conventional photon echo coincides with that of the second exciting radiation pulse, and the maximum amplitude of the echo is achieved for coinciding polarizations of both exciting pulses. In particular, if both exciting pulses are linearly polarized along the X-axis, the echo is determined by the following equations:

$$e_x^{\mathrm{e}}(t') = e_0 \exp(-2\gamma\tau) g(t'-\tau)\,, \quad e_y^{\mathrm{e}}(t') = 0\,, \tag{14}$$

where the function

$$g(t'-\tau) = \int_{-1}^{1} \mathrm{d}z\, G(z, t'-\tau) \tag{15}$$

describes the temporal shape of a conventional echo pulse. However, for mutually orthogonal polarizations of exciting pulses $\mathbf{l}_2\mathbf{l}_1^* = 0$, the two signals formed by the transitions $m_a = 0 \to m_b = -1$ and $m_a = 0 \to m_b = 1$ interfere destructively, so the conventional echo completely disappears. In this case, the echo signal only arises due to elastic depolarizing collisions, leading to the transfer of coherence between different magnetic sublevels of the resonant levels, and is represented by the off-diagonal elements of the resolution matrix of Eqn (6). Such an echo, induced by collisions, was predicted in [17]. In the general case of mutually orthogonal elliptical polarizations, the circular components of two polarization vectors of exciting pulses can be set using a single real parameter α:

$$l_{1,q} = \cos(\alpha)\delta_{q,-1} - \sin(\alpha)\delta_{q,1}\,, \tag{16}$$

$$l_{2,q} = \sin(\alpha)\delta_{q,-1} + \cos(\alpha)\delta_{q,1}\,. \tag{17}$$

The value $\alpha = 0$ corresponds to circular orthogonal polarizations — the first pulse is polarized along the right circle $l_{1,q} = \delta_{q,-1}$, the second, along the left circle $l_{2,q} = \delta_{q,1}$; the value $\alpha = \pi/4$ corresponds to linear orthogonal polarizations — the first pulse is polarized along the X-axis, and the second, along the Y-axis. After substituting Eqns (16) and (17) into (13), and choosing two orthogonal unit vectors $\mathbf{s}_n$ as polarization vectors $\mathbf{l}_n$ of the exciting pulses, we obtain

$$e_n^{\mathrm{c}}(t') = \frac{e_0}{2}\exp(-2\gamma\tau)\left|\sinh\left(\frac{\lambda\tau}{2}\right)\right|^2 \sin(2\alpha) g_{\mathrm{c}}(t'-\tau) l_n^{\mathrm{c}}\,, \tag{18}$$

where the function

$$g_{\mathrm{c}}(t'-\tau) = \int_{-1}^{1} \mathrm{d}z\, G(z, t'-\tau)(1-z^2)^2 \tag{19}$$

describes the temporal shape of the photon echo induced by collisions, and the unit vector $\mathbf{l}^{\mathrm{c}}$ with components

$$l_1^{\mathrm{c}} = -\sin(2\alpha)\,, \quad l_2^{\mathrm{c}} = \cos(2\alpha) \tag{20}$$

represents its polarization.

As follows from Eqn (20), the intensity of the photon echo induced by collisions depends on the ellipticity α of the exciting pulses; it is maximum for linear mutually orthogonal polarizations of exciting radiation pulses $(\alpha = \pi/4)$ and vanishes for circular orthogonal polarizations $(\alpha = 0)$. This result can be explained by the fact that, in the case of circular polarizations of exciting pulses, symmetry is preserved with respect to rotation around the pulse propagation direction (around the Z-axis), so integration over velocity angles ϕ yields a zero for the photon echo intensity, while for linear polarizations of exciting pulses, this symmetry is broken, and after integration over the angles ϕ, nonzero terms remain that provide the echo signal.

In the general case of elliptically polarized pulses of exciting radiation, the echo polarization does not coincide with either the first or the second exciting pulse. It also follows from Eqn (20) that, in the case of linear polarizations of the exciting pulses $(\alpha = \pi/4)$, the collision-induced photon echo signal is linearly polarized, and its polarization coincides with that of the first exciting pulse, whereas in the case of a conventional photon echo its polarization coincides with that of the second exciting pulse.

2.4 Dependence of the collisional photon echo on some experimental parameters

We now consider the amplitude of the collisional photon echo $|e_x^{\mathrm{c}}(\tau)|$ formed by two linearly and mutually orthogonally polarized pulses of resonant radiation $(\mathbf{l}_1 = \mathbf{l}_x,\ \mathbf{l}_2 = \mathbf{l}_y,$ $\alpha = \pi/4)$ and the amplitude of the conventional echo $|e_x^{\mathrm{e}}(\tau)|$ formed by two equally linearly polarized pulses $(\mathbf{l}_1 = \mathbf{l}_2 = \mathbf{l}_x)$ at the time $t' = \tau$, when the echo amplitudes are maximum. It follows from assumption $|\lambda| \ll \gamma$ that for delays $\tau \leqslant 1/\gamma$ the inequality $|\lambda|\tau \ll 1$ holds, so

$$\sinh\left(\frac{\lambda\tau}{2}\right) \approx \frac{\lambda\tau}{2}\,,$$

and the amplitude of the collisional echo should increase in proportion to $(\lambda\tau)^2$. In the opposite limit $\tau \gg 1/\gamma$, the amplitude of the collisional echo decays according to the law $\exp(-2\gamma\tau)$, as for a conventional photon echo. Taking into account the fact that the experiment records the signal power proportional to the square of the electric field strength, we have the limiting cases of small delays τ with increasing power of the collision echo $P^{\mathrm{c}} \propto (\lambda\tau)^4$, while in the limit of large delays both the conventional echo $P^{\mathrm{e}} \propto \exp(-4\gamma\tau)$ and collisional echo $P^{\mathrm{c}} \propto \exp(-4\gamma\tau)$ are attenuated.

Note that experiments to study the collisional echo can be carried out in two ways. The pressure of the buffer gas can be varied, i.e., the anisotropy parameter of collisional relaxation λ can be increased concurrently with the variation in parameter γ, in which case this value should include not only the radiative decay of levels but also the collisional broadening of the line, for example, due to collisions in which phase is lost or translational motion velocity changes due to collisions. The second option is to only vary the delay between exciting pulses τ, i.e., record photon-echo kinetics.

2.5 Experimental results

Everywhere below the intercombination transition ^{174}Yb $^1S_0$ $(6s^2) \leftrightarrow {}^3P_1$ (6s6p) is considered. The upper level of this transition is sufficiently distant from the neighboring levels of the triplet, and the absence of nuclear spin in this isotope guarantees the absence of a hyperfine structure in the transition, so this transition corresponds to the 0–1 type. The experiments used a natural mixture of ytterbium isotopes, in which the content of the ^{174}Yb isotope is 31.84% [18]. The closest absorption lines in the spectrum correspond to even isotopes of ytterbium with atomic masses 172 (detuning +1 GHz), 176 (detuning −955 MHz relative to the above-mentioned ^{174}Yb transition), and 170 (detuning +4196 MHz) and do not have a hyperfine structure [18]. The absorption lines of odd ytterbium isotopes, which are closest in spectrum to the chosen ^{174}Yb transition and have a hyperfine structure, correspond to ytterbium isotopes with masses 171 (detuning −2131 MHz) and 173 (detuning −2389 MHz) [18]. In our experiments, the spectral width of the laser pulses did not exceed 100 MHz [16], so in this case we were working with the isolated transition ^{174}Yb $^1S_0$ $(6s^2) \leftrightarrow {}^3P_1$ (6s6p); other ytterbium isotopes could not be excited by radiation resonant with this transition and could only act as buffer particles.

The first results on detecting a collisional echo [19] were obtained in a mixture of ytterbium vapor with krypton as a buffer gas. However, the anisotropy of collisional relaxation should manifest itself more noticeably as the mass of the buffer atoms becomes greater, and therefore xenon was subsequently used as a buffer gas.

The experimental setup [20], which is described in detail in [16, 21], is shown in Fig. 3. The source of radiation resonant to the ^{174}Yb transition was a pulsed rhodamine-110 dye laser at a radiation wavelength of 555.6 nm, pumped by an excimer XeCl laser with the following parameters: radiation wavelength of 308 nm, pulse duration of 10 ns, and pulse energy of 50 mJ. The dye laser consists of a master oscillator with a short (10-cm) resonator and two amplification stages. In each of these devices, a laminar flow of an alcoholic dye solution is supplied. The master oscillator resonator is formed by a grating of 1800 lines mm^{-1}, which is installed according to an autocollimation scheme and operates in the second order of diffraction, and an output dielectric mirror. The grating is placed in a pressure chamber with adjustable nitrogen pressure, which enables smooth variation of the master oscillator frequency. Downstream from the master oscillator, an additional spectral selector is installed, which is a 1200-line-mm^{-1} diffraction grating. Between the master oscillator and the first amplification stage and between the amplification stages, spatial-angular selectors are installed, each of them is an afocal system of two positive lenses with a diaphragm between them. The central part of the beam at the output of the last amplifier stage is cut out by a diaphragm

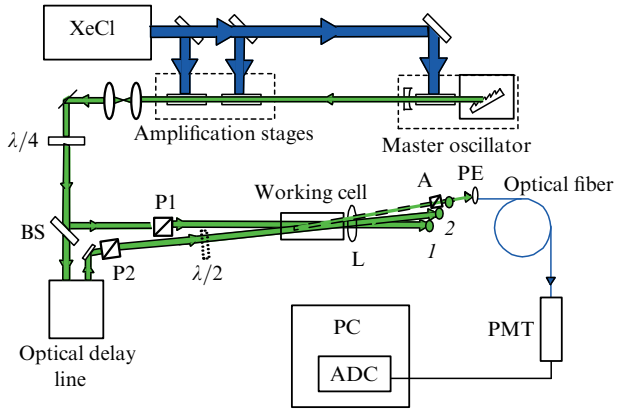

Figure 3. Scheme of the experimental setup for detecting collisional PE. XeCl is the pumping laser; dye laser master oscillator and radiation amplification stages are shown; $\lambda/4$ is a quarter wave plate; BS is translucent plate; $\lambda/2$ is a half-wave plate; PC is a personal computer; and ADC is an analog-to-digital converter of PE signals.

1.5 mm in diameter; the light beam is then expanded by a Kepler telescope to a diameter of 10 mm. This beam enters an external optical circuit. The use of spatial-angular selectors and a telescopic expander made it possible to reduce the background from dye superradiation and form a radiation beam with a fairly uniform transverse intensity distribution and a divergence close to the diffraction limit. The temporal shape of the radiation pulse was smooth without any noticeable fluctuations. Intensity fluctuations were taken into account during data collection and processing.

The output radiation of the dye laser, which is linearly polarized, was converted by a quarter-wave plate ($\lambda/4$ in Fig. 3) into circularly polarized radiation. Resonant radiation pulses, inducing a response from the medium in the form of a photon echo, were formed using a beam splitter plate (BS in Fig. 3) and an optical delay line from a single dye laser pulse. Each of the exciting pulses, separated by delay τ, passed through a Glan–Taylor prism (polarizer P1 or P2 in Fig. 3), which sets linear polarization with a given orientation. Deviation from linear polarization was assessed based on the power of optical radiation of the residual transmission of the prism polarized orthogonally to the main radiation flux; this power did not exceed 10^{-3} of the maximum pulse power. To rotate the polarization plane by 90°, a half-wave plate was used (shown by dashes in Fig. 3). To form the signal of a collisional photon echo, the polarizations of the exciting pulses were set linear and mutually orthogonal. The beams of the first and second pulses propagated in a heated cell containing ytterbium vapor and a buffer gas (in this case, xenon), at an angle of about 2×10^{-3} rad to each other (labelled with numbers 1 and 2 after the working cell in Fig. 3). The magnitude of the angle exceeds the diffraction divergence of the exciting radiation beams and at the same time does not have a noticeable effect on the amplitude of the recorded useful signals. This arrangement of angular photon echo made it possible to spatially separate the weaker photon echo signal from exciting pulse signals. The photon echo signal was detected by a high-speed, high-sensitivity photomultiplier tube (PMT), so it was important to avoid illumination of the detector by exciting radiation pulses, and it was the angular echo setup that made it possible.

Experiments [21] reported the sensitivity of the polarization of the photon echo signal to the longitudinal magnetic

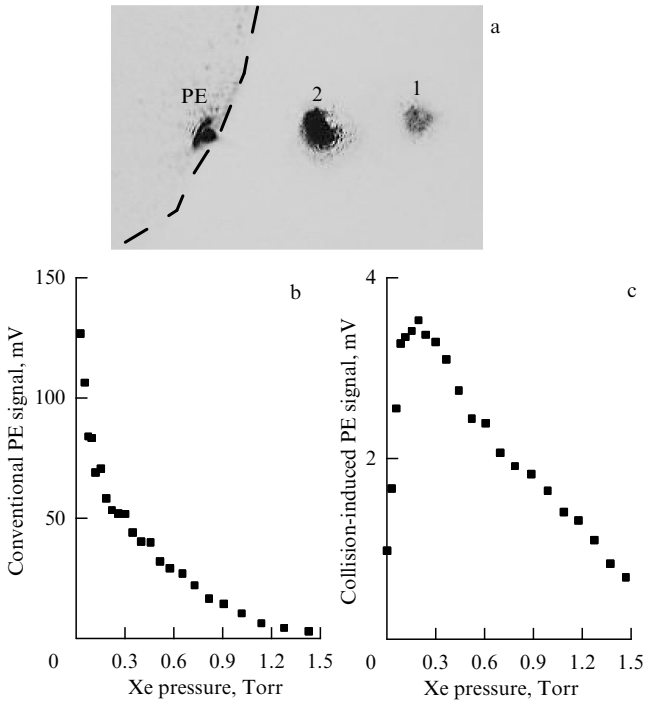

Figure 4. (a) Image recorded by a computer camera; numbers 1 and 2 denote exciting radiation beams, which pass through a neutral light filter, the boundaries of which are shown by the dashed line; the PE signal partially passes through a light filter, so its spatial distribution is distorted. (b, c) Signals of conventional PE (b) and collision-induced PE (c) as a function of the pressure of the xenon buffer gas.

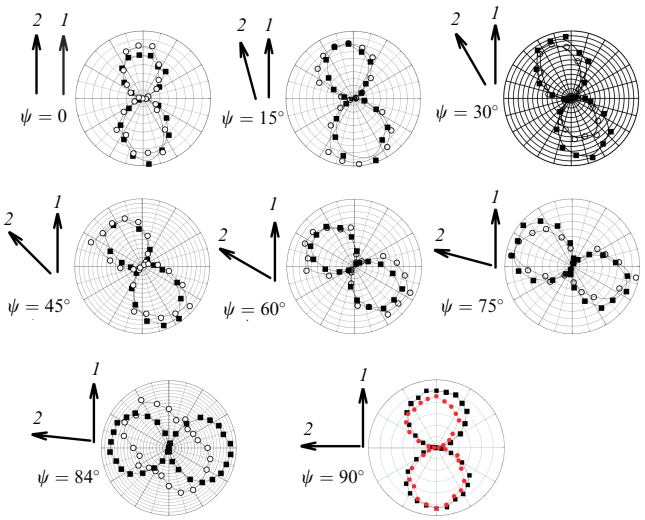

Figure 5. Polarization patterns of a photon echo (experimental points are indicated by circles) formed by two pulses of resonant radiation polarized linearly with an angle ψ between the polarization vectors. For angles $\psi = 0-84°$, dark squares show the polarization patterns of the second pulse; for an angle $\psi = 90°$, those of the first pulse. A transition from a conventional PE, the polarization of which coincides with that of the second exciting pulse, to a collisional PE polarized along the first exciting pulse is seen.

field. In this experiment, special efforts were taken to ensure a zero magnetic field in the working cell, including compensation for the parasitic laboratory field. Echo signals were detected using a photomultiplier, followed by digitization of the signal using a high-speed ADC and accumulation of the photon echo signal. Only those echo signals that were generated by light pulses with power fluctuations of no more than 0.1 of the maximum value were taken into account.

Figure 4a shows the image recorded by a computer camera; numbers 1 and 2 label beams of exciting radiation. The beams pass through a neutral light filter, the boundaries of which are shown by the dashed line; the PE signal partially passes through a light filter, so its spatial distribution is distorted. To obtain the image, a photodiode matrix of a portable web camera without a lens with VGA (640×480) resolution was used. The plots displayed in Fig. 4b, c show the dependence of the signal of a conventional PE (b) and collision-induced PE (c) on the pressure of the xenon buffer gas. For a conventional PE, a monotonic attenuation of the signal is observed with increasing pressure of the buffer gas due to collisions involving a change in the velocity of active atoms. For a collision-induced echo, the signal dependence is nonmonotonic, featuring a rapid increase at low buffer gas pressures and decay at higher buffer gas pressures. The dependences displayed in Fig. 4 give some idea of the relative level of signals from conventional and collisional PEs: the level of the former is two to three orders of magnitude higher. It should also be noted that the collisional-PE signal exists even at zero pressure of the buffer gas. This is due to the fact that the concentration of ^{174}Yb vapors in the natural mixture of isotopes is about 32%, and ytterbium atoms of other isotopes can operate as buffers.

The polarization properties of a PE formed by two pulses of resonant radiation, polarized linearly with an angle ψ between the polarization vectors, were studied in [22] for a gas mixture, the composition of which at given delay τ was close to the maximum of the collisional-echo signal (Xe pressure is ~ 232 mTorr, ytterbium vapor pressure at 567 °C is ~ 12.9 mTorr). Figure 5 shows the results of recording polarization diagrams (the power of the recorded signal is plotted along the radius; the angle is determined by the position of the analyzer); the error in measuring angles did not exceed $\pm1°$; the maximum values of the photon echo were normalized to unity. For each point of each plot, at least 100 measurements were made, from which 25–30 measurements were selected that correspond to the most stable values of the exciting pulse power (data with deviations in the exciting pulse power of more than $\pm10\%$ were not taken into account).

In Fig. 5, black squares mark points on the polarization diagrams of the exciting pulses; the lines connecting them correspond to B-spline interpolation. For the range of angles $\psi = (0-84)°$, these are the diagrams of the second exciting pulse of resonant radiation, while for the angle $\psi = 90°$, the first pulse. For zero angle ψ, the conventional PE is almost two orders of magnitude greater than the maximum recorded signal of the collisional PE. For angles between the polarization vectors of the exciting pulses $\psi = (0-75)°$, the polarization of the recorded signal virtually coincides with that of the second exciting pulse; under such conditions, the signal of conventional PE predominates, and the signal of collisional PE is small. For the angle between the polarization vectors $\psi = 84°$, a complex shape of the polarization diagram of the echo response is visible, the symmetry axis of which does not coincide with that of the diagram of the second exciting pulse. For the indicated angle between the polarization vectors of the exciting pulses, the contributions to the overall response from the conventional and collisional PE can be expected to be of the same order of magnitude. The polarization diagram

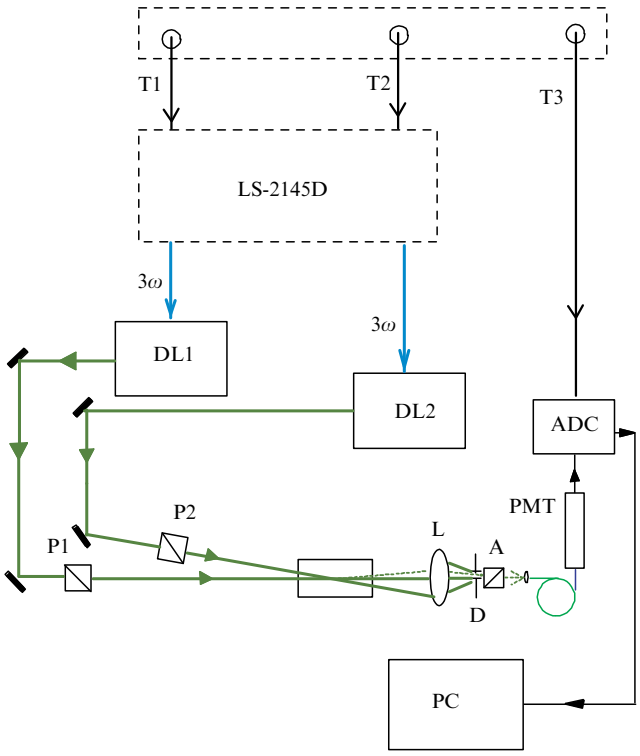

Figure 6. Scheme of the experimental setup for recording the kinetics of collisional PE. LS-2145D is the pump laser that generates a pair of infrared radiation pulses with an adjustable delay between them followed by conversion to the third harmonic for pumping two dye lasers DL1 and DL2; triggers T1 and T2 of a multichannel pulse generator are shown, which trigger pump pulses, along with the T3 trigger, which launches the ADC to process the collisional-PE signal. Conventionally shown in an external setup are two polarizers P1 and P2, a working cell with a mixture of ytterbium with buffer gases, a setup for isolating the collisional-PE signal by an angular echo scheme using a diaphragm D, a polarization analyzer A, a detector of radiation PMT, an ADC, and a PC.

in this case is close to the elliptical type, and this implies that there is a phase difference between the electric fields of the conventional and collisional PE also induced by depolarizing collisions. Finally, for an angle $\psi = 90°$, the polarization diagram corresponds to linear polarization oriented along the first exciting radiation pulse. In this case, the conventional PE completely disappears, and the collisional PE acquires the greatest value (registered 'at zero level').

To study the kinetics of collisional PE [23], an advanced setup was developed that made it possible to vary both parameters: the pressure of the buffer gases and the delay between exciting radiation pulses. A schematic diagram of this installation is shown in Fig. 6.

Used as sources of the two pulses of exciting resonant radiation were the lasers of an original design based on Coumarin-153 dye with optical pumping by the third harmonic of radiation from a pulsed Nd^{3+}:YAG laser (model LS-2145D-C3/2, pulse duration of about 10 ns, manufactured by LOTIS, Belarus). The LS-2145D-C3/2 laser provided a pair of infrared pulses with an adjustable delay between them, followed by third harmonic generation in two KDP crystals. To increase the pump radiation power, *Q*-switching with electro-optical modulators was used. The setup made it possible to vary in 10-ns steps the delay between radiation pulses resonant with the transition of ytterbium atoms ^{174}Yb $^1S_0$ $(6s^2) \leftrightarrow {}^3P_1$ (6s6p). The optical design of the dye lasers included a master oscillator and two amplification stages. Coarse tuning of the emission frequency of each dye laser to the ytterbium transition under study was carried out by rotating the diffraction grating of the master oscillator and fine tuning by changing the nitrogen pressure in the chamber in which the diffraction grating is located. An external setup for generating photon echo signals directed beams into a cell with ytterbium vapor at a small angle (no more than 2 mrad) using several flat mirrors; this made it possible to spatially separate the weak echo response from the strong forming radiation pulses. The polarization of each pulse was set by a polarizer. Analyzer A was located in front of the recording device (PMT), which made it possible to additionally protect the PMT from illumination by the radiation of the second exciting pulse. The polarization of the pulses was linear with an accuracy of at least 10^{-3} in terms of radiation power. In studying a conventional photon echo, the polarizations of the exciting pulses were identical and coincided with the orientation of the analyzer in front of the photomultiplier. For the experiments studying collision-induced PE, the polarization of the second exciting pulse was orthogonal to that of the first, and the orientation of the analyzer coincided with the polarization orientation of the first exciting pulse. Special attention was also paid in this experiment to compensation for Earth's magnetic field and the laboratory magnetic field. The delay between the exciting radiation pulses was set by an external multichannel generator in steps of 10 ns, while the exact value of the delay between optical pulses was measured using attenuated light pulses detected by the photomultiplier. The minimum delay values available in the experiment (50–60 ns) were limited by the features of the recording system. The duration of the exciting pulses was 10 ns, and the lasing linewidth of the dye lasers was on average less than 1 GHz, which is comparable to the Doppler absorption linewidth of ^{174}Yb at the experimental temperature. Presumably, the experimental conditions corresponded to a type intermediate between the formation of a photon echo on a narrow and a wide spectral line. The temperature of the working cell in experiments with pure ytterbium (a natural mixture of isotopes) varied within the 810–860 K range; the ytterbium vapor pressure varied from 5 to 21.5 mTorr. The cell temperature was 860–890 K in experiments where ytterbium was diluted with inert gases. The buffer gas pressure varied from zero to 300 mTorr in mixtures with ytterbium. At maximum buffer gas pressure, the dilution of ^{174}Yb atoms was as high as 1:30. A number of noble gases, He, Ne, Ar, Kr, and Xe, with natural isotope contents were used as buffer atoms; collisions of ^{174}Yb atoms with each other and with atoms of other ytterbium isotopes were also studied.

Figure 7 shows the experimental kinetic curves for a photon echo induced by collisions in pure ytterbium at a pressure of 21.5 mTorr (curve *1*, squares), for a mixture of 21.5 mTorr Yb + 90 mTorr Ar (curve *2*, triangles) and for a mixture of 21.5 mTorr Yb + 101 mTorr Xe (curve *3*, dots). Solid curves in Fig. 7 show approximation under the assumption $|\lambda|\tau \ll 1$ according to the formula for the power of the collision photon echo $P_{\mathrm{col}PE} \propto (|\lambda|\tau)^4 \exp(-4\gamma\tau)$. In pure ytterbium, a segment of an increasing echo signal is visible for delays less than 80 ns; the maximum is clearly observed. With a further increase in delays, the collision echo fades.

In mixtures with lighter gases, the region of the maximum of the collision photon echo signal is less visible. Figure 8

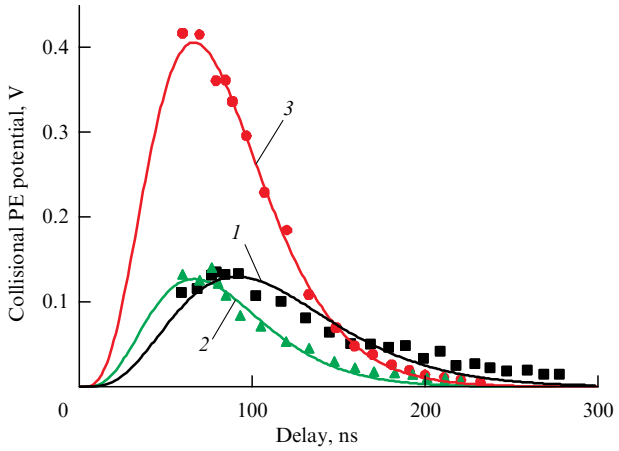

Figure 7. Kinetic curves of collisional PE in pure ytterbium (*1* — squares), in a mixture with argon (*2* — triangles), and in a mixture with xenon (*3* — dots).

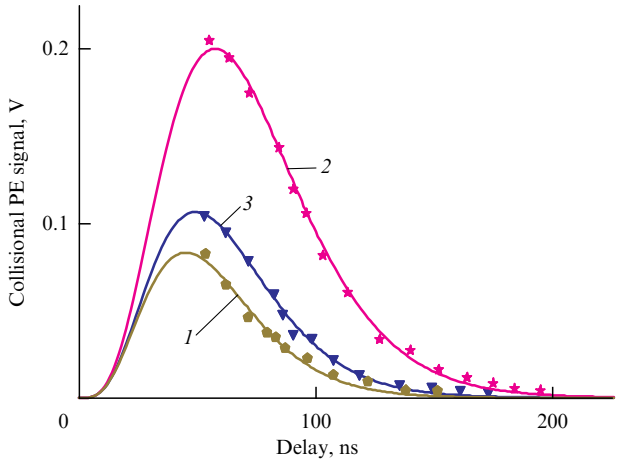

Figure 8. Kinetic curves of collisional PE in mixtures of ytterbium with helium (curve *1*, pentagons), neon (curve *2*, stars), and krypton (curve *3*, triangles).

shows the kinetic curves of collision echo decay for mixtures 46.4 mTorr Yb + 201 mTorr He (curve *1*, pentagons); 46.4 mTorr Yb + 195 mTorr Ne (curve *2*, stars); and 46.4 mTorr Yb + 203 mTorr Kg (curve *3*, triangles). Solid curves are the result of approximation according to the dependence of the collision echo power on the parameters $|\lambda|$, τ, and γ described above. Values $|\lambda|$ were fitting parameters; the delays τ were specified in the experiment and additionally controlled; and the pressure-dependent relaxation rates γ were determined from the kinetic decay curves of the conventional echo, which coincided with the decay of the collisional echo.

Table 1 shows decay rate constants of a conventional photon echo $d\gamma/dp$ in units of 10^7 s^{-1} Torr^{-1}, determined from six pressure points of each buffer gas with a step of 50 mTorr in the range of 0–300 mTorr.

For mixtures of ytterbium with buffer gases, the segment of the maximum signal of the collisional echo is not determined very definitely, so the results for mixtures with noble gases were not used to estimate the anisotropy parameter of collisional relaxation, in contrast to the kinetic curves in pure ytterbium. For pure ytterbium vapor, experiments to record the kinetics of conventional and collisional PE (one kinetic curve is shown in Fig. 7) were carried out under the same conditions. The ratio of the maximum signal amplitudes for conventional and collisional PE for each ytterbium pressure can be used to determine the value of $|\lambda|/\gamma$, and the anisotropy parameter itself $|\lambda|$ is found from the measured decay rates of the photon echo γ. The parameter $|\lambda|$ was estimated for the ytterbium vapor pressure p ranging from 13.9 to 21.5 mTorr. This range was determined by the recording conditions (for pressures below 13.9 mTorr, the collisional echo is too weak, while at pressures above 21.5 mTorr, it is not possible to carry out experiments without a buffer gas due to the risk of the cell windows being covered with an ytterbium film).

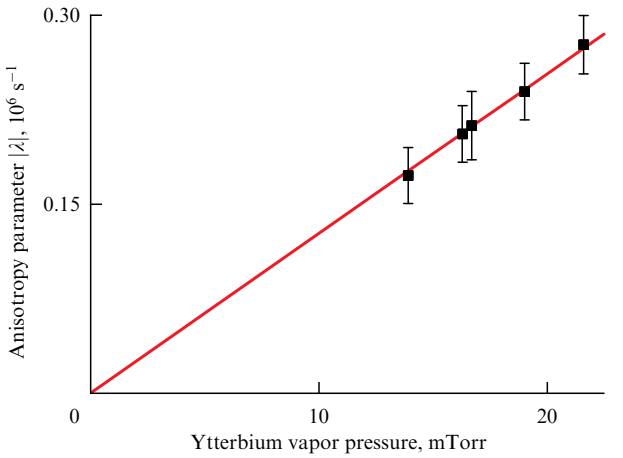

Figure 9. Parameter of collisional relaxation anisotropy increases with increasing ytterbium vapor pressure.

Table 1. Decay rate constants of a two-pulse photon echo (10^7 s^{-1} Torr^{-1}).

Buffer atom	$d\gamma/dp$
He	2.57 ± 0.33
Ne	2.63 ± 0.26
Ar	2.62 ± 0.27
Kr	3.09 ± 0.35
Xe	3.31 ± 0.41
Yb	5.77 ± 1.41

The plot of $|\lambda|(p)$ is displayed in Fig. 9, where an increase in the anisotropy parameter with increasing ytterbium pressure can be seen. The corresponding collisional relaxation anisotropy constant is $d|\lambda|/dp = (1.27 \pm 0.14) \times 10^7$ s^{-1} Torr^{-1}. Taking into account the value of γ in pure ytterbium, we obtain the estimate $|\lambda|/\gamma = 0.22 \pm 0.07$.

3. Stimulated photon echo at the transition 0–1

Among many coherent nonstationary phenomena, it is the stimulated photon echo (SPE) that attracts attention from the point of view of both applied research, which relates to optical (or phase) memory, and basic research into the details of collisional interaction in a gaseous medium, in particular, depolarizing collisions [5, 6]. Most applications are based on SPE polarization properties. However, the polarization properties of SPE formed on such a relatively simple transition as 0–1 have not been studied before. Our research carried out in 2012–2021 filled this gap.

3.1 Experimental studies of SPE polarization properties at the transition 0–1

Our first studies of SPE at the transition ^{174}Yb ($6s^2$) $^1S_0 \leftrightarrow$ (6s6p) $^3P_1$ [24, 25] used radiation from a rhodamine-110 dye laser pumped by the second harmonic of an Nd^{3+}:YAG laser (model LS-2137U, Belarus). The laser comprised a master oscillator and three amplification stages similar to that used in [21]. Coarse tuning of the laser frequency was carried out by rotating the diffraction grating (DG in Fig. 10a) and tilting the Fabry–Perot interferometer (FP) in the master oscillator, while fine tuning was done by changing the pressure of dry nitrogen gas in the chamber containing these elements. To remove the fluorescence of cells containing dye, spatial filtration of the laser beam was used.

The output laser radiation was linearly polarized; it was split by translucent plates into three beams, two of which passed through optical delay lines to form the second and third exciting radiation pulses. All three beams were directed into a working cell with ytterbium vapor in a noncoplanar geometry — along three edges of a pyramid with small angles (about 2×10^{-3} rad) at the apex (Fig. 10b). This angular SPE geometry made it possible to spatially isolate a weak SPE signal and protect the detector from powerful exciting pulses.

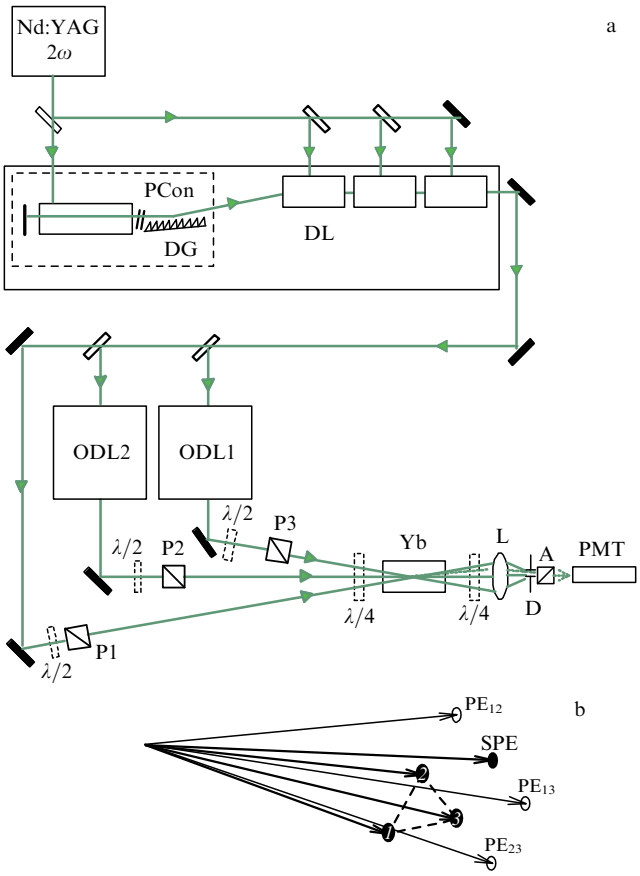

Figure 10. (a) Scheme of the experimental setup for studying SPE polarization. LS-2137U is a pump laser that generates the second harmonic of radiation for pumping a dye laser DL: two optical delay lines, ODL1 and ODL2; polarizers P1–P3 are shown; half-wave plates $\lambda/2$ were used when it was necessary to rotate the linear polarization of radiation by 90°; quarter-wave plate $\lambda/4$ shown by the dashed line in front of the cell with ytterbium (Yb) vapor made it possible to convert linear polarizations into circular ones; the same plate downstream from the cell made it possible to reverse polarization transformation. The angular scheme of SPE formation (b) made it possible to spatially separate the SPE signal using diaphragm D; analyzer A was used to analyze the polarization of SPE signals.

The setup shown in Fig. 10a is fairly simple and provides maximum overlap of all three exciting resonant radiation pulses. The duration of the exciting radiation pulses was $T_1 = T_2 = T_3 = 8$ ns; the delay between the first and second pulses was $\tau_{12} = 22$ ns, and between the second and third pulses it was $\tau_{23} = 20$ ns. The SPE signal emerged approximately 22 ns after the end of the third pulse.

To form an SPE with three linearly polarized radiation pulses, half-wave plates were placed in each of the beams (the first and the other two that passed through the delay line), which made it possible to create sequences of excitation pulses of the following types: ↑↑↑ identical linear polarizations of the three pulses, ↑→↑ with crossed polarization of the second pulse, and ↑↑→ with crossed polarization of the third pulse. Before carrying out the experiments, the degree of polarization and the orientation of the polarization diagram of each exciting pulse were checked by rotating analyzer A, located downstream from the working cell in front of the photomultiplier; the SPE polarization diagram was recorded similarly.

To obtain the required combinations of circular polarizations, first, sequences of linear polarizations of exciting pulses were created in which the polarization patterns of the exciting pulses were controlled as described above. Then, a quarter-wave plate was located as close as possible to the input window of the cell with gas; due to the small angle between the vectors of the exciting pulses, one plate was sufficient to convert linear polarizations into circular ones. Downstream from the working cell with the gas under study, a second quarter-wave plate was placed, which made it possible to clearly distinguish right- and left-handed polarizations of exciting pulses and SPE signals using polarization diagrams.

To obtain undistorted results on SPE polarization, Earth's magnetic field and the laboratory magnetic field were compensated for to a level of no more than 20×10^{-3} G. Deviations of the exciting pulse polarization from the linear one did not exceed 10^{-3} in terms of radiation power.

The working cell temperature was maintained at about 840 ± 2 K; the buffer gas pressure was varied in 50-mTorr steps in the range of 0–300 mTorr.

The laser radiation frequency was maintained at the center of the intercombination transition ($6s^2$) $^1S_0 \leftrightarrow$ (6s6p) $^3P_1$ of ^{174}Yb atoms with an accuracy of about 100 MHz.

Signals from three exciting radiation pulses, the SPE signal, and some double-pulse PEs could be observed using a camera located in the focal plane of lens L after the last quarter-wave plate. The SPE signal, spatially separated from the exciting radiation beams according to the synchronism rule $\mathbf{k}_{SPE} = \mathbf{k}_1 + \mathbf{k}_2 - \mathbf{k}_3$ (here, $\mathbf{k}_{SPE}$ is the SPE wave vector and $\mathbf{k}_i$, $i = 1, 2, 3$, are the wave vectors of the exciting pulses), could be isolated using diaphragm D placed instead of the camera in the region of the focal plane of the lens collecting signal to the photomultiplier.

3.2 SPE polarization properties at the transition 0–1 in pure ytterbium: linear polarizations of exciting pulses

Figure 11 shows the properties of the SPE formed in ytterbium vapor at the transition ^{174}Yb $^1S_0$ ($6s^2$) $\leftrightarrow$ $^3P_1$ (6s6p) by three pulses of linearly polarized resonant radiation.

If all three excitation radiation pulses have the same linear polarization, the SPE signal is polarized in the same

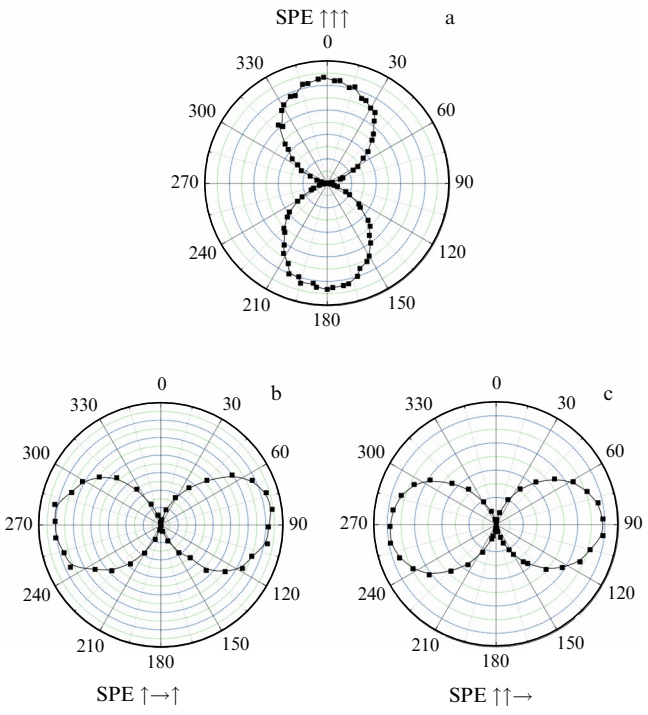

Figure 11. Polarization patterns of the SPE formed by three exciting pulses of resonant radiation of the same linear polarization of the SPE↑↑↑ (a); polarization of the second exciting pulse is orthogonal to the remaining SPE pulses ↑→↑ (b); polarization of the third exciting pulse is orthogonal to the remaining SPE pulses ↑↑→ (c). In the last two cases, the SPE polarization coincides with the 'crossed' polarization of the exciting pulse.

way. The corresponding polarization diagram is presented in Fig. 11a.

If one of the exciting pulses is polarized linearly and orthogonally to the other two exciting pulses, the SPE polarization at the $0 \leftrightarrow 1$ transition in pure ytterbium is linear and coincides with the polarization of this pulse with 'crossed' polarization. This can be seen in two polarization diagrams: the diagram in Fig. 11b designated SPE↑→↑ (in the notation, the pulses follow from left to right) corresponds to the case where the second pulse of exciting radiation has crossed polarization; the diagram in Fig. 11c designated SPE↑↑→ corresponds to the case where the third pulse of exciting radiation has a crossed linear polarization.

It should be noted that sequences of exciting impulses of the form ↑↑→ (crossed third impulse) and →↑↑ (crossed first impulse) are not equivalent. In pure ytterbium, a stimulated SPE→↑↑ echo is not formed. Apparently, the first exciting impulse plays a special role in the formation of SPE.

3.3 Collision-induced SPE at the transition 0–1

The polarization properties of SPE presented in Section 3.2 are consistent with theoretical results [26] for the $0 \leftrightarrow 1$ transition. Study [26] took into account the influence of depolarizing collisions to predict the occurrence of SPE exclusively due to depolarizing collisions for the case of polarizations of exciting →↑↑ impulses. The existence of this collisional SPE is due [26] to the difference in the relaxation rates of the alignment and orientation of the upper operating level of the 0–1 transition.

It was shown experimentally in [24] that, if a gas mixture of ytterbium vapor with a buffer gas Xe is excited by a sequence of resonant radiation pulses with a combination of polarizations →↑↑, a collisional SPE signal is actually observed, the polarization of which coincides with the polarization of the first exciting radiation pulse crossed with linearly polarized second and third pulses (Fig. 12). The power of this signal nonmonotonically depends on the buffer gas pressure. The maximum value of the collisional SPE in the mixture is attained at a xenon pressure of 200×10^{-3} Torr; in this case, the ytterbium vapor pressure was $\approx 7.5 \times 10^{-3}$ Torr, i.e., the dilution of ytterbium was significant. With a further increase in xenon pressure, the collisional SPE decays, as can be seen in Fig. 12.

3.4 SPE polarization properties at the transition 0–1 in pure ytterbium: circular polarizations of exciting pulses

Experimental data [25] displayed in the diagrams in Fig. 13 were obtained for SPE formed by exciting pulses of various combinations of circular polarization: (rrr), (rlr), and (rrl). In all cases, the diagrams were recorded after converting the SPE signal with a quarter-wave plate located downstream from the working cell in front of the detector. For all of the above combinations of circular polarizations of exciting pulses, the SPE polarization coincides with the polarization of the exciting pulse oriented orthogonally to the others.

The addition of a buffer gas to ytterbium in the case of SPE formed by circular pulses of the form (rrr), (rlr), and (rrl) led to a monotonic decrease in the SPE signals.

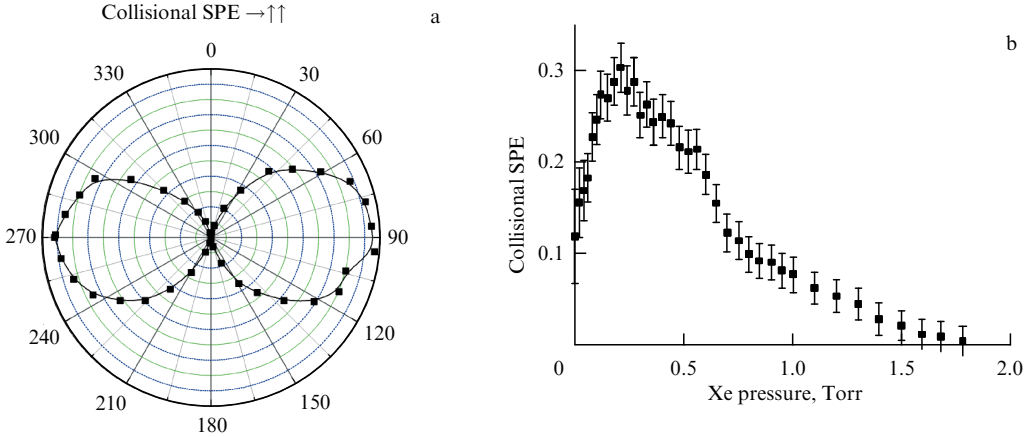

Figure 12. (a) Polarization pattern of a collisional SPE formed by a sequence of linearly polarized pulses →↑↑ and (b) dependence of echo power on the buffer gas pressure.

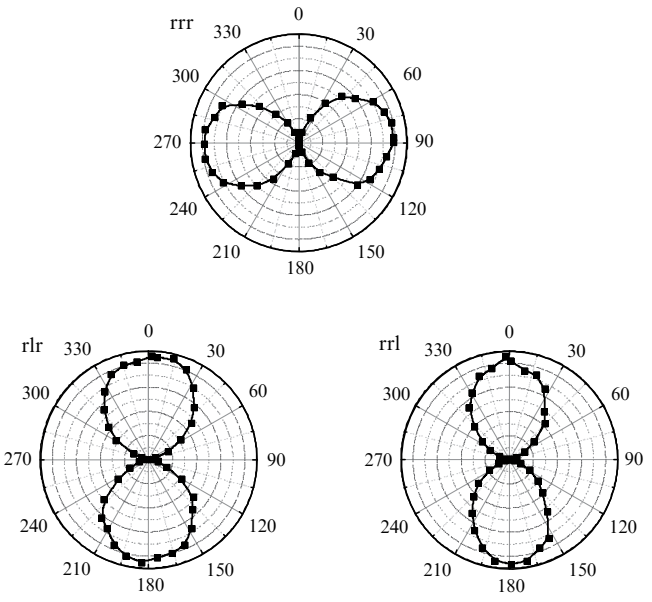

Figure 13. Polarization patterns of an SPE formed by exciting pulses with various combinations of circular polarization (rrr), (rlr), and (rrl). They coincide with the polarization of the exciting pulse polarized orthogonally to the others. All polarization patterns were recorded after conversion by a quarter-wave plate located downstream from the working cell in front of the detector.

Note that the combination of polarizations of exciting (lrr)-type pulses did not lead to the formation of SPE up to a level of 10^{-5} of the power of the exciting pulses. Dilution of ytterbium vapors also failed to result in the formation of collision SPE. This result differs from the case of $\rightarrow\uparrow\uparrow$ exciting pulses, when dilution with a buffer gas resulted in the formation of a collisional SPE.

3.5 SPE technique in studying depolarizing collisions

The SPE signal depends not only on delays between the exciting pulses and their amplitudes and durations (i.e., on the area of each ith pulse θ_i — the integral of the Rabi frequency over time) but also on the polarization of each pulse and the relaxation rates of each magnetic sublevel. Calculations of SPE taking into account the degeneracy of levels [5, 14] revealed that it is convenient to pass from the populations of magnetic sublevels to the moments of atomic levels: population $\gamma^{(0)}$, orientation $\gamma^{(1)}$, alignment $\gamma^{(2)}$, and higher moments. Moreover, it was shown in [5, 14] that for all types of transitions the main contribution to the SPE signal is made by these three lowest polarization moments of the upper and lower levels. For the transition 0–1, the relaxation rates of population $\gamma^{(0)}$, orientation $\gamma^{(1)}$, and alignment $\gamma^{(2)}$ represent the full set of the rates of upper-level relaxation due to depolarizing collisions.

The electric field strength of the photon echo signal is determined from Maxwell's equations [5]:

$$\mathbf{e}^{\mathrm{e}}(t') \propto \int_{-\infty}^{\infty} \mathrm{d}v\, f(v) \exp\left[-\mathrm{i}kv(t'-\tau_{12})\right]\mathbf{F}\,, \tag{21}$$

$$\mathbf{F} = C_1 S_1 S_2 S_3 \sum_{\kappa=0}^{2} \mathbf{f}^{(\kappa)} \exp\left(-\gamma^{(\kappa)}\tau_{23}\right), \tag{22}$$

where $k = \omega/c$, $t' = t - z/c - T_1 - \tau_{12} - T_2 - \tau_{23} - T_3$, and $f(v)$ is the distribution function over projections v of the velocity of atoms onto the Z-axis,

$$S_n = \frac{\theta_n}{\Omega_n} \sin\left(\frac{\Omega_n}{2}\right), \quad D_n = \exp\left(\frac{\mathrm{i}kvT_n}{2}\right), \tag{23}$$

$$C_n = \cos\left(\frac{\Omega_n}{2}\right) + \mathrm{i}\,\frac{kvT_n}{\Omega_n} \sin\left(\frac{\Omega_n}{2}\right), \tag{24}$$

$$\Omega_n = \sqrt{\theta_n^2 + (kvT_n)^2}\,, \tag{25}$$

and T_n and θ_n are the duration and area of the nth pulse, respectively. The quantities $\mathbf{f}^{(\kappa)}$ depend in a complex way on the areas and polarizations of the exciting pulses. In the special case $\psi_1 = \psi_2 = \psi$,

$$f_x^{(0)} = \frac{4}{3}\, C_2 C_3^*\,, \quad f_x^{(2)} = \frac{1}{6}\, C_2 C_3^* \big(1 + 3\cos(2\psi)\big), \tag{26}$$

$$f_y^{(2)} = \frac{1}{2}\, C_2 D_3^* \sin(2\psi)\,, \quad f_x^{(1)} = f_y^{(1)} = f_y^{(0)} = 0\,, \tag{27}$$

and in the case $\psi_2 = -\psi_1 = \psi$,

$$f_y^{(0)} = 0\,, \quad f_y^{(1)} = \frac{1}{2}\, D_2 D_3^* \sin(2\psi)\,, \tag{28}$$

$$f_y^{(2)} = \frac{1}{2}\,(C_2 - D_2) D_3^* \sin(2\psi)\cos(2\psi)\,. \tag{29}$$

Thus, if $\psi_1 = \psi_2 = \psi$ ($\psi \neq 0$ and $\psi \neq \pi/2$), the decay of the e_y^{e} component of the echo signal, orthogonal to the polarization vector of the third exciting pulse, with increasing time interval τ_{23} will be determined by only the alignment relaxation rate $\gamma^{(2)}$. The dependence of the echo amplitude on the areas of exciting pulses during the formation of an echo on a narrow spectral line ($kuT_n \ll 1$, where $u = \sqrt{2k_{\mathrm{B}}T/m}$ is the average thermal velocity, and m is the mass of the ytterbium atom) has the form

$$e_y^{\mathrm{e}} \propto \sin\theta_1 \sin\theta_2 \sin\frac{\theta_3}{2}\,. \tag{30}$$

At $\psi_2 = -\psi_1 = \pi/4$, the decay of the e_y^{e} component of the echo signal will be determined by only the orientation relaxation rate $\gamma^{(1)}$, while the dependence of the echo amplitude on the areas on a narrow spectral line has the form

$$e_y^{\mathrm{e}} \propto \sin\theta_1 \sin\frac{\theta_2}{2} \sin\frac{\theta_3}{2}\,. \tag{31}$$

Finally, if $\psi_1 = \psi_2 = (1/2)\arccos(-1/3)$, the decay of the e_x^{e} component of the echo signal, parallel to the polarization vector of the third exciting pulse, will be determined only by the population relaxation rate $\gamma^{(0)}$, while the dependence of the echo amplitude on areas on a narrow spectral line has the form

$$e_x^{\mathrm{e}} \propto \sin\theta_1 \sin\theta_2 \sin\theta_3\,. \tag{32}$$

Such significantly different dependences (30)–(32) are due to the fact that the echo signals at the 0–1 transition are formed with the participation of three states: the ground state and two magnetic sublevels $m = -1$ and $m = +1$ of the excited state. In this system, similar to that of three nondegenerate levels of the V-configuration, three exciting pulses can form different types of echo (stimulated, three-level, and collisional) [26] with different dependences on the areas of these pulses of the form (30)–(32), and the contribu-

Table 2. Selection of polarization angles ψ_1 and ψ_2 of exciting pulses and SPE polarization components measured to find relaxation rates $\gamma^{(0)}$, $\gamma^{(1)}$, and $\gamma^{(2)}$.

ψ_1 and ψ_2	SPE component	Rate
$\psi_1 = \psi_2 = \psi$ ($\psi \neq 0, \psi \neq \pi/2$)	$\perp \mathbf{e}_3$	$\gamma^{(2)}$
$\psi_1 = -\psi_2 = \pi/4$	$\perp \mathbf{e}_3$	$\gamma^{(1)}$
$\psi_1 = \psi_2 = (1/2)\arccos(-1/3)$	$\parallel \mathbf{e}_3$	$\gamma^{(0)}$

tion of each type of echo to the total signal depends on the polarizations of the exciting pulses. When experimentally determining each of the relaxation rates (population, orientation, or alignment), the optimal areas of exciting pulses corresponding to the maximum intensities of echo signals should be selected individually taking into account dependences (30)–(32).

The calculated dependence of the measured intensities of the SPE polarization components on the exciting pulse areas is as follows: $I \propto \sin\theta_1 \sin\theta_2 \sin(\theta_3/2)$ for $\gamma^{(2)}$ being measured; $I \propto \sin\theta_1 \sin(\theta_2/2) \sin(\theta_3/2)$ for $\gamma^{(1)}$ being measured; and, if $\gamma^{(0)}$ is measured, $I \propto \sin\theta_1 \sin\theta_2 \sin\theta_3$. These formulas give an idea of the sensitivity of SPE signals to the intensities of exciting pulses.

Thus, the rate of population $\gamma^{(0)}$, orientation $\gamma^{(1)}$, and alignment $\gamma^{(2)}$ decay due to depolarizing collisions can be determined using the dependence on the delay τ_{23} of the SPE signal generated by three pulses of resonant radiation with specially selected angles ψ_1 and ψ_2 between polarization vectors of the first and, consequently, second pulse relative to that of the third pulse. For a $0 \leftrightarrow 1$ transition, a possible choice of angles ψ_1 and ψ_2 and the SPE polarization component is presented in Table 2.

3.6 Technique for registering SPE kinetics

The experimental setup for recording the SPE kinetics as a function of the delay between the second and third exciting pulses is shown in Fig. 14. Three light pulses, resonant to the transition ^{174}Yb $(6s^2)\ ^1S_0 \leftrightarrow (6s6p)\ ^3P_1$, were formed in study [27] in two dye lasers using optical pumping by the third harmonic of a two-channel Nd^{3+}:YAG laser, LOTIS (model LS-2145D-C3/2, Minsk, Belarus). The delay between two pump laser channels could be varied over a wide range in 10-ns steps by triggering the channels from an external generator. The light pulse from the first dye laser was split by a translucent mirror into two parts, one of which passed through a mirror spatial delay line. Thus, the first dye laser generated two light pulses with a fixed delay of 33 ns between them. Both of these radiation pulses featured a high degree of mutual coherence. The third light pulse was generated in the second dye laser. Its delay relative to the first two pulses, which varied in the experiment in the range of 50–550 ns, was provided by an external generator that controlled the launch of pump laser pulses. The delay was checked using the PMT signal from residual illumination by all three pulses, and this value was used to plot kinetic curves. To decrease PMT illumination by exciting pulses, an angular SPE scheme was used, in which the wave vectors of all radiation beams that form the SPE signal are directed along the edges of a tetrahedron, and angles between them do not exceed 2×10^{-3} rad.

The duration of all exciting radiation pulses was 10 ns. The area of each exciting radiation pulse is estimated as 10π, obtained based on measurements of the pulse energy, its duration, and the transverse distribution of the radiation

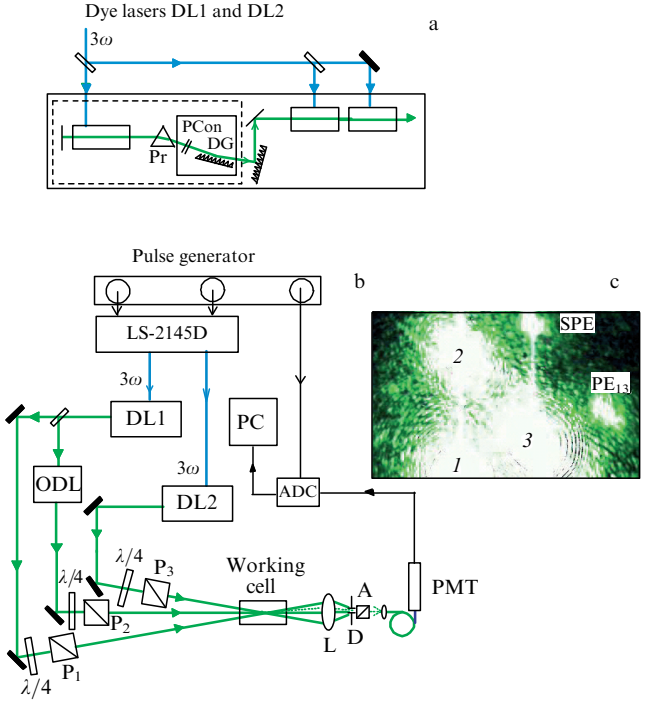

Figure 14. Scheme of an experimental setup for studying an SPE kinetics (a) setup of dye lasers DL1 and DL2; (b) pulse generator generating two pump pulses; optical delay line ODL downstream from the splitter, forming the second exciting pulse; all three pulses are brought together in the working cell at small angles to each other. (c) Image made by a web camera placed in the focal plane of the lens L downstream from the cell instead of the diaphragm; numbers indicate the centers of the exciting pulse beams; SPE and PE signals from pulses *1* and *3* are visible. In the process of measurements, the SPE radiation beam was separated by diaphragm D. Desired polarization component was selected by analyzer A, focused by a microlens onto a piece of fiber and recorded by the PMT. Required sequence of polarizations of exciting pulses was created by a combination of quarter-wave plates $\lambda/4$ and polarizers P_1, P_2, and P_3.

beams. It was arrived at by assuming a uniform distribution of light energy over the cross section of the radiation beam. In reality, this distribution is not uniform and may differ for each of the three pulses and from shot to shot. In the registration program for the ADC, the SPE signal from each shot can be observed without averaging, in the so-called oscilloscope mode. It is seen that for some shots the echo signal is large, while for others it is very small. Thus, the area value of 10π is the average effective value of the exciting pulse areas, which turned out to be optimal for averaging over a large number (100–300) of measurements. The stability of the specified value was maintained in the process of averaging by rejecting the measurements that correspond to the deviations of the amplitudes of exciting pulses exceeding 10%.

The wavelength of both dye lasers was controlled with an accuracy of 0.0001 nm using a special meter developed using five Fabry–Perot interferometers. If the carrier frequencies of the dye laser radiation deviated from each other by more than 150 MHz, the corresponding measurements were rejected. In the experiment, each point on the plots was obtained as a result of averaging over 300 or more measurements. The laser emission wavelength was maintained at 555.802 nm, and the spectral width of the light pulses was 150 MHz. To obtain such a spectral width of the emission line, a Fabry–Perot interferometer was introduced into the resonator (including a dielectric mirror, a glass prism, and a diffraction grating of

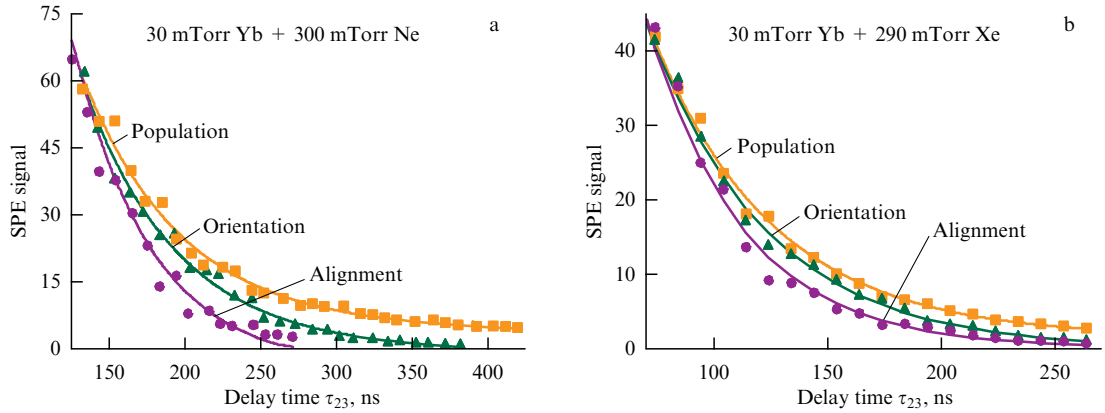

Figure 15. SPE signals showing the decay of population, orientation, and alignment in mixtures of ytterbium with neon (a) and xenon (b).

1200 lines mm^{-1} operating in the grazing incidence mode) of each of the two master dye lasers. Additional diffraction gratings of 1200 lines mm^{-1} were installed between each master oscillator and the first amplification stage.

The temperature in the ytterbium cell, which was controlled using a platinum–rhodium thermocouple, was maintained at 600 °C with an accuracy of 1°. The saturated vapor pressure of ytterbium at this temperature is ~ 30 mTorr. The pressure of the inert buffer gases (He, Ne, Ar, Kr, Xe) in the cell was maintained at a level of 50-400 mTorr, which guaranteed domination of the collisions of active ytterbium atoms with buffer gas atoms.

To select the polarization angles of the exciting pulses, the radiation of each exciting beam with the initial linear polarization was passed through a quarter-wave plate for conversion to circular polarization, and further through a Glan–Taylor prism to select the required polarization vector of each exciting pulse. To register the required SPE component, an analyzer was located in front of the signal detector (PMT). The radiation polarization downstream from the Glan–Taylor prisms and the analyzer was linear with an accuracy of no worse than 10^{-3} in terms of radiation power.

To measure the orientation decay rate $\gamma^{(1)}$, polarization angles of ±45° were used. The power of the echo polarization component orthogonal to the polarization vector of the third pulse was measured in accordance with Table 2. To measure the decay rate of population $\gamma^{(0)}$ and alignment $\gamma^{(2)}$, the same angles ψ_1 and ψ_2, approximately equal to 55°, were used in the experiment, and the powers of SPE polarization components both parallel and orthogonal to the polarization vector of the third exciting pulse were also measured in accordance with Table 2. In this case, the parallel component of the echo decays as population, and the orthogonal component, as alignment. The choice of angles ψ_1 and ψ_2 presented above preserved the adjustment conditions for measuring the decay rates of population and alignment, which made it possible to directly compare the magnitude of the signals and the two decay rates. In measuring the orientation decay rate, it was necessary to correct the adjustment, since the angular excitation setup is very sensitive to any rotations of the optical elements (to change the direction angle of the polarization vector of the first and second pulses, two pass-through optical elements were rotated, namely, the phase plate and Glan–Taylor prism). Several independent measurements were carried out for each gas; the results were reproducible on a daily basis.

3.7 Studies of depolarizing collisions of ytterbium atoms with inert gas atoms

Curves representing the dependence of the SPE component parallel or orthogonal to the polarization vector of the third exciting pulse on the delay time fit fairly accurately to the decaying exponential for all angles ψ_1 and ψ_2 used and for all partners in collisions of ^{174}Yb atoms with buffer gases. An example of kinetic curves is shown in Fig. 15.

The measured rates of collisional relaxation in the $\gamma^{(i)}$ population, orientation, and alignment of the $^3P_1$ level of ^{174}Yb atoms increased linearly with increasing buffer gas pressure. These dependences are displayed in Fig. 16.

For light buffer gases, He, Ne, and Ar, the rate of collisional decay of orientation almost coincides with the population decay rate; the difference often does not exceed the measurement error. For heavier buffer gases Kr, Xe, the difference among the three relaxation constants $\gamma^{(0)}$, $\gamma^{(1)}$, and $\gamma^{(2)}$ becomes more significant.

In a series of measurements of $\gamma^{(i)}(p)$ for all buffer gases, the ytterbium vapor pressure was the same, ~ 30 mTorr; therefore, all $\gamma^{(i)}(p)$ plots converge at zero pressure to the values measured in pure ytterbium vapor without an admixture of buffer gases. These measured values, which are shown in all plots displayed in Fig. 16, are $\gamma^{(0)}(0) = 0.24$, $\gamma^{(1)}(0) = 0.26$, and $\gamma^{(2)}(0) = 0.34$ in units of 10^6 s^{-1}. The points where the straight lines approximating the $\gamma^{(i)}(p)$ dependences cross the ordinate axis are somewhat different for different buffer gases. These approximation results presented in the same units of measurement yield the following values: for He, 0.27, 0.27, 0.30; for Ne, 0.25, 0.27, 0.31; for Ar, 0.25, 0.26, 0.32; for Kg, 0.25, 0.27, 0.35; and for Xe, 0.30, 0.33, 0.39. Given the accuracy of measurements of each $\gamma^{(i)}(p)$ value shown in the plots of Fig. 16, the disagreement between the approximation and measurements without buffer gases can be considered satisfactory.

The dependences of the relaxation rates $\gamma^{(i)}$ on the buffer gas pressure can be used to determine the relaxation constants $d\gamma^{(i)}/dp$ (here, $i = 0, 1, 2$, and p is the buffer gas pressure) for each buffer gas. These results are presented in Table 3.

According to the values displayed in Table 3, for light buffer gases He, Ne, and Ar, $d\gamma^{(0)}/dp$ and $d\gamma^{(1)}/dp$ almost coincide, while for heavier buffer gases, Kr and Xe, the difference among the three relaxation constants $d\gamma^{(0)}/dp$, $d\gamma^{(1)}/dp$, and $d\gamma^{(2)}/dp$ is larger. The tendency is also clearly seen towards an increase in all three decay rate constants of the $^3P_1$ level of ^{174}Yb atoms with increasing mass of the buffer gas.

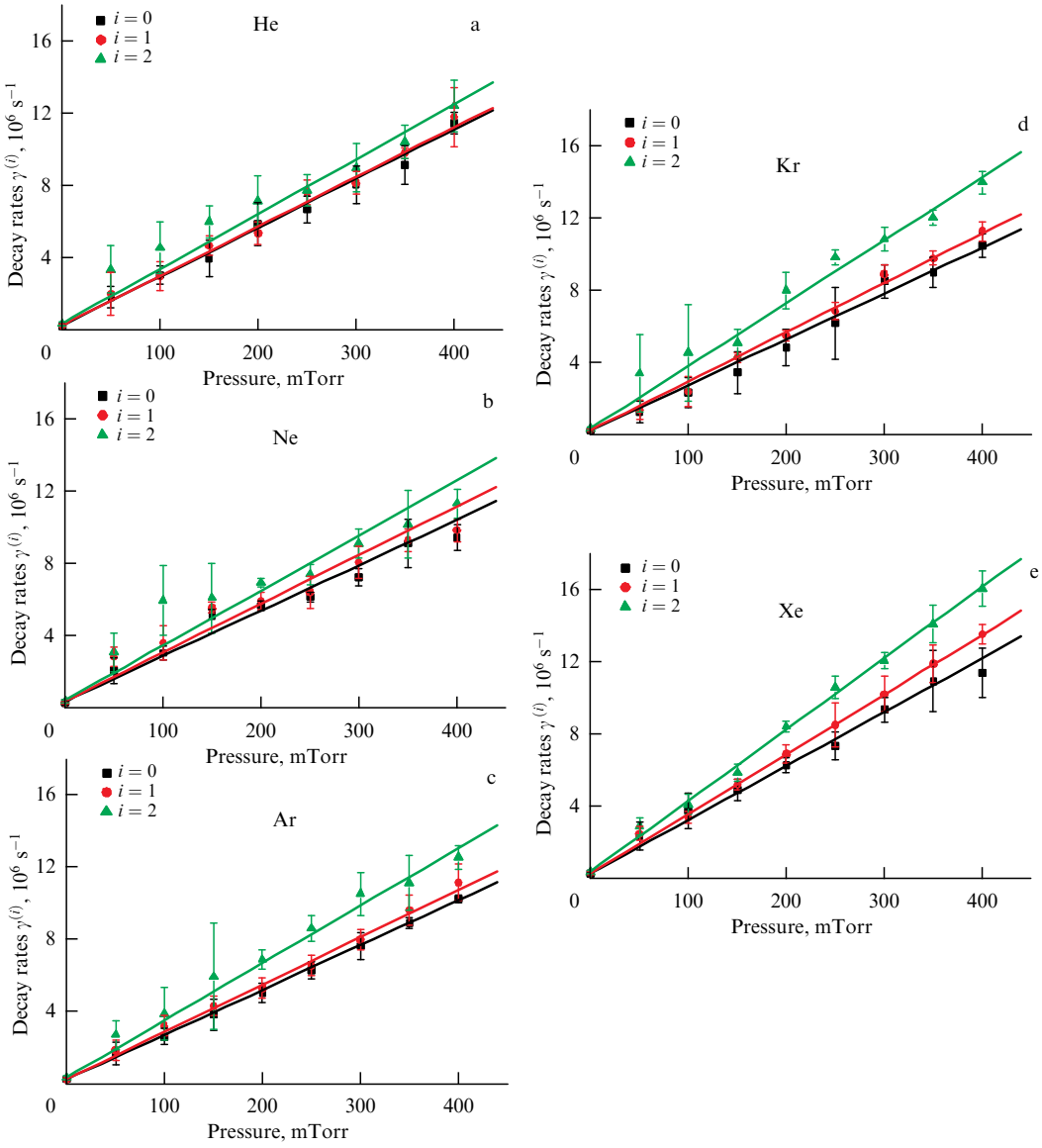

Figure 16. Signal relaxation rates $\gamma^{(i)}$ showing the decay of population, orientation, and alignment in mixtures of ytterbium with He (a), Ne (b), Ar (c), Kr (d), and Xe (e).

Table 3. Measured relaxation rate constants (10^7 s^{-1} Torr^{-1}).

Buffer gas	$d\gamma^{(0)}/dp$	$d\gamma^{(1)}/dp$	$d\gamma^{(2)}/dp$
He	2.72 ± 0.12	2.75 ± 0.12	3.04 ± 0.18
Ne	2.52 ± 0.13	2.71 ± 0.13	3.05 ± 0.15
Ar	2.49 ± 0.11	2.62 ± 0.11	3.17 ± 0.13
Kr	2.54 ± 0.14	2.73 ± 0.14	3.48 ± 0.18
Xe	2.98 ± 0.13	3.30 ± 0.11	3.95 ± 0.11

The clear-cut dependence $\gamma^{(0)}(p)$ observed in the experiment for all buffer gases suggests the presence of an elastic process that reduces the amplitude of the stimulated photon echo regardless of the polarizations of the light pulses that form it. Such a process indeed exists: this is elastic scattering with a change in velocity (velocity changing collision), and its rate, apparently, should increase with increasing pressure of the buffer gas.

It can be assumed that the measured dependences $\gamma^{(0)}(p)$ are most likely due to velocity changing collisions $\gamma^{(0)}(p) = \gamma_{vcc}(p)$. Following this logic, to isolate the contribution of purely depolarizing collisions (relaxation of the orientation $\Gamma^{(1)}$ or alignment $\Gamma^{(2)}$), it is necessary to subtract the dependences $\gamma_{vcc}(p)$ from the measured dependences $\gamma^{(1)}(p)$ and $\gamma^{(2)}(p)$. Table 4 presents the relaxation rate constants due to elastic velocity changing collisions $d\gamma_{vcc}(p)/dp$ and the relaxation rate constants for orientation $d\Gamma^{(1)}/dp$ and alignment $d\Gamma^{(2)}/dp$.

Table 4. Rate constants of relaxation due to velocity changing collisions $d\gamma_{vcc}/dp$, orientation $d\Gamma^{(1)}/dp$, and alignment $d\Gamma^{(2)}/dp$ in units of 10^7 s^{-1} Torr^{-1}.

Buffer gas	$d\gamma_{vcc}(p)/dp$	$d\Gamma^{(1)}/dp$	$d\Gamma^{(2)}/dp$
He	2.72 ± 0.12	0.03 ± 0.12	0.32 ± 0.18
Ne	2.52 ± 0.13	0.19 ± 0.13	0.53 ± 0.15
Ar	2.49 ± 0.11	0.13 ± 0.11	0.68 ± 0.13
Kr	2.54 ± 0.14	0.19 ± 0.14	0.94 ± 0.18
Xe	2.98 ± 0.13	0.32 ± 0.11	0.97 ± 0.11

Table 4 clearly shows that the measurement accuracy is low in the case of light buffer gases. Nevertheless, the values

of the orientation relaxation constants $d\Gamma^{(1)}/dp$ exhibit an increasing dependence on the buffer gas mass; for alignment relaxation constants $d\Gamma^{(2)}/dp$, this dependence is more pronounced. The dependence $d\gamma_{vcc}(p)/dp$ has the same character: it increases with increasing mass of the buffer gas.

4. Discussion

Based on the studies conducted, it can be argued that collisions of active atoms with atoms of the surrounding buffer gas can influence in a nontrivial way the photon echo formed at the optical transition of active particles. An example of such an influence of collisions is the photon echo induced by the anisotropy of relaxation during collisions, i.e., the dependence of the relaxation rate of the transition dipole moment on the velocity vector of the translational motion of active particles. In the section devoted to the theoretical analysis of the collisional photon echo, the expansion of the dipole moment in the direction along the velocity of translational motion of active atoms and across this velocity is introduced. If we take the reference frame of an atom moving with velocity $\mathbf{v}$, the gas of buffer particles acquires velocity $-\mathbf{v}$ in the direction along the velocity of the active atom. If the relaxation rate depends on the absolute value of the velocity of the relative motion of the active atom and buffer particles, the relaxation rate will be greater. However, no additional drift velocity of the buffer particles arises in the transverse direction, and the relaxation rate does not change. This is the well-known 'wind effect,' or anisotropy of collisional relaxation; references to theoretical studies can be found in [20]. The use of the spectroscopic 0–1 transition in combination with the described experimental methods made it possible to examine the influence of the anisotropy of collisional relaxation 'at the base level' in the absence of other phenomena. Indeed, in the atomic gas ^{174}Yb at the transition $(6s^2)\ ^1S_0 \leftrightarrow (6s6p)\ ^3P_1$, two pulses of resonant exciting radiation polarized linearly and mutually orthogonally, in the absence of collisions with buffer atoms do not excite a photon echo, but if diluted with a buffer gas a collisional-echo signal is formed [20]. The amplitude of such a collisional PE depends in a nonmonotonic way on the buffer gas pressure, and its polarization differs from that of the photon echo formed without collisions. The study of the kinetics of the echo [23] induced by the anisotropy of collisional relaxation made it possible to estimate the parameters of the anisotropy of collisional relaxation of ytterbium atoms.

A nontrivial influence of collisions was also discovered for the SPE — in the form of the SPE induced by depolarizing collisions. This coherent response arises solely due to the nonzero difference between the relaxation rates of alignment and orientation. The observation of this phenomenon 'in its pure form,' in the absence of a conventional SPE, was carried out for the ^{174}Yb $(6s^2)\ ^1S_0 \leftrightarrow (6s6p)\ ^3P_1$ transition when an optical transition is excited by a combination of linearly polarized resonant radiation pulses, the second and third pulses having linear polarization crossed with the first. Under such excitation conditions, the SPE signal does not emerge in a pure gas of active atoms. If diluted with a buffer gas, a collision-induced SPE appears with a nonmonotonic dependence of the amplitude on the buffer gas pressure and with linear polarization parallel to that of the first exciting pulse [24]. The behavior of this signal in a weak magnetic field (0–0.4 G) suggests the inequality $\gamma^{(2)} > \gamma^{(1)}$ [28], while a comparison of the plot of the collisional SPE dependence on the magnetic field strength with the calculated dependence allows an estimation of the difference $\gamma^{(2)} - \gamma^{(1)}$ [29, 30]. Unfortunately, in the mentioned studies on the dependence of collisional SPE signals on the strength of a weak magnetic field, only a few values of the difference in relaxation rates were obtained by fitting the shape of the experimental curve to the theoretical dependence. More detailed studies of collisional SPE in a weak longitudinal magnetic field could presumably enable progress in measuring the relaxation of level polarization moments.

As noted in the Introduction, the influence of elastic collisions involving a change in the translational motion velocity should be manifested in the decay of both PE and SPE. This is also evidenced by a comparison of the data displayed in Table 1 and the second column from the left in Table 4 for collisions of ^{174}Yb atoms with noble gas atoms. For ease of comparison, we present them in the form of a separate table (Table 5).

Table 5. Comparison of PE decay rate constants $d\gamma/dp$ and one of the SPE decay characteristics $d\gamma^{(0)}(p)/dp = d\gamma_{vcc}(p)/dp$ in the same units 10^7 s^{-1} Torr^{-1}.

Buffer atom	$d\gamma/dp$	$d\gamma_{vcc}(p)/dp$
He	2.57 ± 0.33	2.72 ± 0.12
Ne	2.63 ± 0.26	2.52 ± 0.13
Ar	2.62 ± 0.27	2.49 ± 0.11
Kr	3.09 ± 0.35	2.54 ± 0.14
Xe	3.31 ± 0.41	2.98 ± 0.13

Indeed, the obtained values of the PE relaxation rate constants $d\gamma/dp$ and the relaxation rate of the upper working level $d\gamma^{(0)}/dp$ determined by the SPE method are fairly close. It is far from apparent that such a significant effect of elastic collisions is due to the use of an angular registration scheme in SPE experiments (recall that the angles between the pulse vectors of the resonant radiation forming the SPE do not exceed 2 mrad). It may be assumed that for the collisional analogues of PE and SPE, the influence of elastic scattering of atoms involving a change in the velocity of translational motion is also unavoidable.

In theoretically describing the shape of the spectral line of atoms, it is customary to take into account collisions that detune the phase of the atom's radiation. In considering the formation of a PE or SPE signal, it is not possible to distinguish the type of collisions in which the phase is lost from elastic collisions with a change in the translational velocity of the active atom, since in both cases the emitting atom is removed from the set of particles that form the coherent response. In elastic scattering, the atom frequency changes from $\omega_0 + kv_z$ to $\omega_0 + kv_z'$ over a time interval called a collision (this can be a time scale of the order of 10^{-13} s), so it is a change in radiation frequency that occurs rather than a dephasing of radiation.

Comparisons of data relating to the rates of collisional decay of orientation and alignment of the upper operating level $(6s6p)\ ^3P_1$ of the ^{174}Yb atom from Table 4 are doubtful since, according to the concept of depolarizing collisions, these velocities (and rate constants) should not differ to this extent. An explanation of the results displayed in Table 4 may be a low accuracy of measurements. An alternative explanation may be that elastic collisions with translational velocity change and depolarizing collisions are not independent, and it

is not adequate to process data by subtracting $d\gamma^{(0)}/dp$ from the data for $d\gamma^{(1)}/dp$ and $d\gamma^{(2)}/dp$.

5. Conclusion

Based on theoretical studies of the photon and stimulated photon echo, which take into account the degeneracy of levels [5, 6, 14, 17, 26], a set of experimental methods has been developed, making it possible to determine the polarization properties of the photon and stimulated photon echo using the example of the 0–1 transition for ^{174}Yb atoms under various experimental conditions.

In studying the phenomena of photon echo and stimulated photon echo formed at the ^{174}Yb $(6s^2)\,{}^1S_0 \leftrightarrow (6s6p)\,{}^3P_1$ transition, the polarization properties of these coherent responses under conditions of weak influence of collisions were established. In the case of strong dilution of active ytterbium atoms with noble gases, the phenomenon of collisional PE, caused by the anisotropy of collisional relaxation, was experimentally discovered, and estimates of the anisotropy parameter were obtained. The phenomenon of collisional SPE, the emergence of which is associated with the difference between the rates of relaxation of orientation and alignment of the upper working transition level, was experimentally studied.

The experimental technique presented here, which is intended for studying depolarizing collisions using the SPE method with specially selected polarizations of exciting radiation pulses, may be useful for other atoms with a similar spectral transition. For the transition ^{174}Yb $(6s^2)\,{}^1S_0 \leftrightarrow (6s6p)\,{}^3P_1$, this method was used to determine the constants of collisional decay of orientation and alignment of the upper working level of the specified transition in collisions with noble gas atoms. A significant contribution of elastic collisions to the decay of SPE signals was discovered. A feature of the PE and SPE methods is their sensitivity to elastic collisions that change the velocity of translational motion of active particles (more precisely, the projection of velocity on the direction of propagation of exciting radiation). In the present study, the emphasis is on depolarizing collisions that change the state of the magnetic sublevels of the atom; it is possible, however, that the PE and SPE methods can be modified to explore the elastic scattering of atoms.

References

1. Kopvillem U Kh, Nagibarov V R *Fiz. Met. Metalloved.* **15** 313 (1963)
2. Kurnit N A, Abella I D, Hartmann S R *Phys. Rev. Lett.* **13** 567 (1964)
3. Manykin E A, Samartsev V V *Opticheskaya Ekho-Spektroskopiya* (Optical Echo Spectroscopy) (Moscow: Nauka, 1984)
4. Allen L, Eberly J H *Optical Resonance and Two-Level Atoms* (New York: Wiley, 1975); Translated into Russian: *Opticheskii Rezonans i Dvukhurovnevye Atomy* (Moscow: Mir, 1978)
5. Yevseyev I V, Yermachenko V M, Samartsev V V *Depolarizing Collisions in Quantum Electrodynamics* (Boca Raton, FL: CRC Press, 2004); Translated from Russian: *Depolyarizuyushchie Stolknoveniya v Nelineinoi Elektrodinamike* (Moscow: Nauka, 1992)
6. Evseev I V, Rubtsova N N, Samartsev V V *Kogerentnye Perekhodnye Protsessy v Optike* (Coherent Transient Processes in Optics) (Moscow: Fizmatlit, 2010)
7. Evseev I V, Rubtsova N N, Samartsev V V *Fotonnoe Ekho i Fazovaya Pamyat' v Gazakh* (Photon Echo and Phase Memory in Gases) (Kazan: Kazan. Gos. Univ., 2009)
8. Pomerantsev N M *Usp. Fiz. Nauk* **65** 87 (1958)
9. Oraevskii A N *Sov. Phys. Usp.* **10** 45 (1967); *Usp. Fiz. Nauk* **91** 181 (1967)
10. Vasilenko L S, Rubtsova N N *Opt. Spectrosc.* **58** 422 (1985); *Opt. Spektrosk.* **58** 697 (1985)
11. Comaskey B, Scotti R E, Shoemaker R L *Opt. Lett.* **6** 45 (1981)
12. Forber R A et al. *Phys. Rev. Lett.* **50** 331 (1983)
13. Carlson N W, Babbitt W R, Mossberg T W *Opt. Lett.* **8** 623 (1983)
14. Evseev I V "Teoriya polyarizatsionnoi ekho-spektroskopii atomov i molekul, vzaimodeistvuyushchikh posredstvom uprugikh depolyarizuyushchikh stolknovenii" ("Theory of polarization echo spectroscopy of atoms and molecules interacting via elastic depolarizing collisions"), Doctoral Dissertation in Mathematics and Physics (Moscow: Moscow Engineering Physics Institute, 1987)
15. Vasilenko L S, Rubtsova N N, in *Lazernye Sistemy* (Laser Systems) (Ed. V N Lisitsyn) (Novosibirsk: Inst. Teplofiziki SO AN SSSR, 1982) p. 143
16. Rubtsova N N et al. *Phys. Rev. A* **84** 033413 (2011)
17. Matskevich V K, Yevseyev I V, Yermachenko V M *Opt. Spectrosc.* **45** 8 (1978); *Opt. Spektrosk.* **45** 17 (1978)
18. Clark D L et al. *Phys. Rev. A* **20** 239 (1979)
19. Rubtsova N N et al. *Laser Phys. Lett.* **3** 353 (2006)
20. Rubtsova N N et al. *JETP Lett.* **87** 103 (2008); *Pis'ma Zh. Eksp. Teor. Fiz.* **87** 110 (2008)
21. Rubtsova N N et al. *Phys. Rev. A* **70** 023403 (2004)
22. Rubtsova N N et al. *Laser Phys.* **19** 171 (2009)
23. Rubtsova N N, Kochubei S A, Khvorostov E B, Reshetov V A *J. Exp. Theor. Phys.* **129** 812 (2019); *Zh. Eksp. Teor. Fiz.* **156** 875 (2019)
24. Khvorostov E B et al. *Laser Phys. Lett.* **10** 036001 (2013)
25. Gol'dort V G et al. *Laser Phys. Lett.* **10** 076002 (2013)
26. Reshetov V A, Popov E N *J. Phys. B* **45** 225502 (2012)
27. Rubtsova N N, Kochubei S A, Khvorostov E B, Reshetov V A *J. Exp. Theor. Phys.* **133** 389 (2021); *Zh. Eksp. Teor. Fiz.* **160** 466 (2021)
28. Khvorostov E B et al. *Laser Phys. Lett.* **11** 126004 (2014)
29. Rubtsova N N et al. *Laser Phys. Lett.* **14** 026001 (2017)
30. Rubtsova N N et al. *Laser Phys. Lett.* **15** 046001 (2018)